

ALMA MATER STUDIORUM - UNIVERSITÀ DI BOLOGNA

SCHOOL OF ENGINEERING

DEPARTEMENT of
ELECTRICAL, ELECTRONIC AND INFORMATION ENGINEERING
“Guglielmo Marconi”
DEI

**MASTER’S DEGREE IN
AUTOMATION ENGINEERING**

MASTER THESIS
in
Modeling and Simulation of Mechatronic Systems

**PI Control of a Piezoelectric Bending Microactuator for
Precision Positioning Applications**

CANDIDATE

Nicole Vignoli

SUPERVISOR

Prof. Alessandro Macchelli

CO-SUPERVISOR

Prof. Hector Ramirez

Academic Year
2022/2023

Session
IV

Acknowledgments

At the end of my studies, there are many people whom I have to thank. First and foremost, my parents, who provided me with the freedom to make my own choices and supported me at all times and in every place, even when I was abroad. I want to express my gratitude to Dad and Mom for allowing me to venture out so many times. Rest assured, I always come back, so there's no need to worry about my future mobility.

I appreciate my grandmother for listening to me while I prepared for exams, even when she had no knowledge of the subject, especially when it was in English.

I extend my thanks to all my relatives for being present in my life.

A special thanks to my friends from Forlì, Bologna, and those I met abroad. There was always someone ready to talk during the most challenging moments, and thanks to all of them, I had some very enjoyable times.

I am grateful to my professors, both Italian and Chilean, for imparting knowledge and providing me with the opportunity to visit Chile. I would also like to acknowledge the Chilean ANID BASAL project FB0008, which enabled me to develop this thesis.

Contents

Abstract	9
Introduction	11
1 From piezoelectric material to piezoelectric actuators	15
1.1 Piezoelectric Material	15
1.2 Piezoelectric Actuators	18
1.2.1 Types of piezoelectric actuators	18
1.2.2 Applications for piezoelectric actuators	21
1.3 Nonlinear behaviour: Hysteresis	25
2 Modelling of Piezoelectric Actuator	27
2.1 Bouc-Wen model	27
2.2 PHS model	29
2.3 Model Identification	31
3 PI Control	35
3.1 Controller Design	35
3.1.1 PI based on sinusoidal response identified model	38
3.1.2 PI based on step response identified model	41
3.1.3 Parameters comparison	42
3.2 Simulations	45
3.3 Global Stability	48
4 Experimental Validation	51
4.1 Experimental Setup	51
4.2 Experimental Tests	57
4.2.1 Step response	57
4.2.2 Trajectory tracking	58
Conclusions	63

List of Figures

1.1	Piezoelectric effect	16
1.2	Inverse piezoelectric effect	16
1.3	Classification of crystals	17
1.4	Bending actuator [1]	19
1.5	Longitudinal actuator [2]	20
1.6	Tube actuator [3]	21
1.7	Piezoelectric micro-thruster	22
1.8	Piezoelectric gripper	23
1.9	Piezoelectric micro-assembly example	24
1.10	Piezoelectric micro-pump	24
1.11	Hysteresis curve	26
2.1	Piezoelectric Actuator Model	28
2.2	Bouc-Wen Hysteresis	29
2.3	Nonlinear damping example	30
2.4	Sinusoidal input response	34
2.5	Hysteresis for sinusoidal input	34
2.6	Step input response	34
3.1	PI controller block diagram	36
3.2	Control System Designer	38
3.3	Control System Designer - PI controller	39
3.4	Control System Designer - Final system with PI controller	40
3.5	Root Locus comparison	41
3.6	Control System Designer - Open loop system	42
3.7	Control System Designer - Closed loop system	43
3.8	Feedforward action	47

3.9	Step response	47
3.10	Sinusoidal response and Hysteresis	48
4.1	Configuration diagram	52
4.2	Experimental setup	52
4.3	HMI - Control Desk	53
4.4	Piezoelectric actuator connection configuration	53
4.5	MicroLabBox	54
4.6	PB4VB2S bender piezoelectric actuator	55
4.7	A400DI amplifier	55
4.8	LK-G87 Keyence sensor head	56
4.9	LK-G3001P Keyence sensor driver	56
4.10	Step response	58
4.11	Sinusoidal response	60
4.12	Hysteresis	61

List of Tables

2.1	PHS model parameters	32
2.2	Bouc-Wen model parameters	33
2.3	Models fit percentages (%)	33
3.1	Model parameters comparison	45

Abstract

The primary focus of this thesis is to develop a control strategy for a piezoelectric bending actuator. This actuator exhibits hysteresis between the driving voltage and the displacement, characterized by high nonlinearity and a noticeable phase shift as the frequency increases. The aim is to design a controller that is easily implementable, incorporating some calculation simplifications. The chosen controller is a PI (Proportional-Integral) controller, widely recognized and utilized in industry.

Two PI controller designs are developed, each considering different model identifications. One model is based on a port-Hamiltonian system identified for sinusoidal response (as studied in [4]), while the other is based on identification for step response. Several tests are presented for both PI controllers, involving both step and sinusoidal input signals at different amplitudes and frequencies.

The testing of the PI controllers on real device was conducted at the Advanced Center of Electrical and Electronic Engineering (AC3E) of the Federico Santa María Technical University (UTFSM) in Valparaíso, Chile, where this thesis was developed. The hardware setup and testing enabled the concretization of the theoretical analysis.

The piezoelectric actuator exhibits different behavior with the two PI controllers. There is no definitive superiority of one controller over the other, but each PI controller performs better when working with the type of response its model identification was based on. This implies that the PI controller designed for the port-Hamiltonian system performs better with sinusoidal input signals, while vice versa for the other PI controller, which works better with step input signals.

Introduction

Nowadays, piezoelectric actuators are widely used due to their high resolution (in the order of micro-meter), compactness, high efficiency, fast response time and high force capability. As the term "piezoelectric" suggests, these actuators are constructed from piezoelectric materials, and their behavior is based on the inverse piezoelectric effect discovered in 1881 by Pierre and Jacques Curie. The inverse effect produces a small displacement on the actuator when voltage is applied. There are various types of piezoelectric actuators differing in shape (bending, longitudinal, tube, etc.) and material (BTO, PZT, etc.). This diversity has enabled the application of piezoelectric actuators in several fields, from aerospace to medicine (for ultra-precise positioning devices), and from industry to daily life devices (such as in our mobile phones). While piezoelectric actuators offer tremendous utility, they come with the disadvantage of exhibiting strong nonlinear input/output behavior, described by hysteresis [5]. Through appropriate control design, it is possible to compensate for such nonlinearity.

This thesis focuses on control design for piezoelectric actuators and it is developed at the Advanced Center of Electrical and Electronic Engineering (AC3E) of the Federico Santa María Technical University (UTFSM) in Valparaíso, Chile [6]. The AC3E is a research center focused on developing innovative solutions and cutting-edge technology in the fields of electrical and electronic engineering. It was established in 2014, and is located at the UTFSM in Valparaíso. The AC3E is supported by the Chilean government's National Commission for Scientific and Technological Research (ANID), as well as private and public sector partners.

The AC3E's mission is to promote excellence in research, development, and

innovation in electrical and electronic engineering, with a particular emphasis on areas that have a high potential for industrial application and social impact. The center brings together leading researchers, academics, and students from various Chilean universities, fostering a multidisciplinary and collaborative research environment.

The thesis presents a PI controller design made for a commercial piezoelectric actuator [7] [8]. The analysis showed are combined to the studies presented in [4], where the same bending actuator is modeled with a port-Hamiltonian system [9]. Consequently, the PI controller analysis is firstly base on such model, through some calculation simplifications. The port-Hamiltonian model identification considers only sinusoidal response of the system. Another identification based on the step response and subsequent PI controller analysis is also presented. The PI controllers found are simulated on Simulink, a MATLAB software, for both step and sinusoidal input signals at different amplitudes and frequencies.

Finally, experimental tests on a real plant are conducted. The hardware setup and regulation are configured to test the PI controllers. The resulting behavior is analyzed and compared with each other.

The thesis is organized in five main chapters:

- **Chapter 1)** Piezoelectric material from its origins to its classification is introduced. The focus then shifts to piezoelectric actuators, detailing various typologies, potential applications, and their nonlinear behavior, the hysteresis;
- **Chapter 2)** Various models for piezoelectric actuators are presented, with a focus on the Bouc-Wen model and the port-Hamiltonian model;
- **Chapter 3)** The control design for a PI controller is explained, featuring the derivation of two PI controllers based on different model identifications, one derived from sinusoidal response and the other from step response. Simulation tests using Simulink and a global stability analysis are conducted;
- **Chapter 4)** The experimental hardware setup is detailed, and the ex-

perimental tests on the real plant for the PI controllers, developed in the previous chapter, are explained;

- **Chapter 5)** Conclusions and comments on future work are provided.

Chapter 1

From piezoelectric material to piezoelectric actuators

The objective of this chapter is to initially explain what a piezoelectric material is, along with its properties, and subsequently, how it is used for actuators. Various types of piezoelectric actuators and potential applications are also presented.

1.1 Piezoelectric Material

Piezoelectricity is described as electric polarization in a substance, especially crystals, resulting from the application of mechanical stress. The term "Piezoelectric" is derived from the Greek "piezein," meaning to squeeze or press, and "piezo," which is Greek for to push.

In 1880, Pierre and Jacques Curie discovered the piezoelectric effect. This effect can be observed in materials with a polar axis without a center of symmetry. Polar axes are those axes of symmetry that cannot be transferred to the opposite direction by symmetry operations. When stress is applied to certain crystal faces of a piezoelectric material, charge centers shift across the crystal, turning it into a dipole. The intensity and direction of charge transfer depend on the direction of compression. The overall phenomenon is referred to as the piezoelectric effect (see Figure 1.1).

Initially known as pyroelectricity, the term "piezoelectricity" was suggested

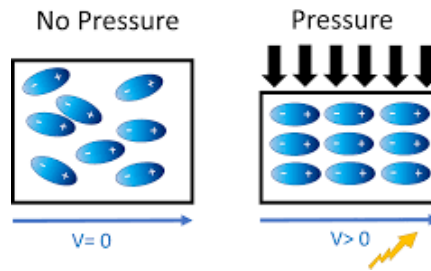


Figure 1.1: Piezoelectric effect

by Hankel in 1881. Later, Lippmann proposed that the inverse piezoelectric effect should also exist. This suggestion was verified by Curie in 1881, confirming the presence of the inverse effect, which is similar to the direct piezoelectric effect. Thus, piezoelectricity can be reversed, leading to what is known as the inverse piezoelectric effect (see Figure 1.2).

The inverse piezoelectric effect involves the production of mechanical deformation in the material when an electric field is applied. The induced mechanical deformation is proportional to the strength of the applied electric field, and the direction of the induced strain can be changed by reversing the polarity of the electric field. This reversible effect is a distinctive characteristic of such materials [10] [11] [12].

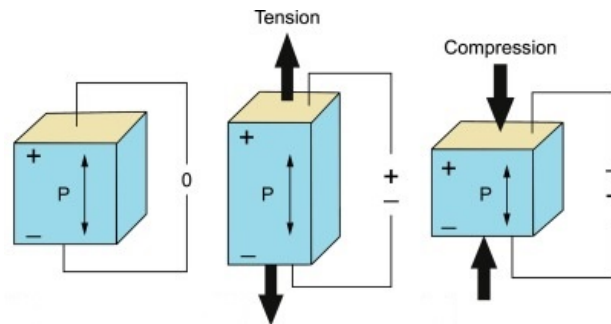


Figure 1.2: Inverse piezoelectric effect

Piezoelectric materials exhibit either a crystal structure or, at least, areas with a crystal-like structure. In general, a crystal is characterized by a periodic repetition of the atomic lattice structure in all directions of space. The smallest repetitive part of the crystal is termed a unit cell. Depending on the symmetry properties of the unit cell, we can distinguish between 32 crystal

classes, also termed crystallographic point groups. Piezoelectric properties only arise when the structure of the unit cell is asymmetric. Out of the 32 crystal classes, 21 are non-centrosymmetric, meaning they do not have a center of symmetry. Among these, 20 crystal classes show piezoelectricity. While 10 crystal classes are pyroelectric, the remaining 10 crystal classes are non-pyroelectric (Figure 1.3) [5].

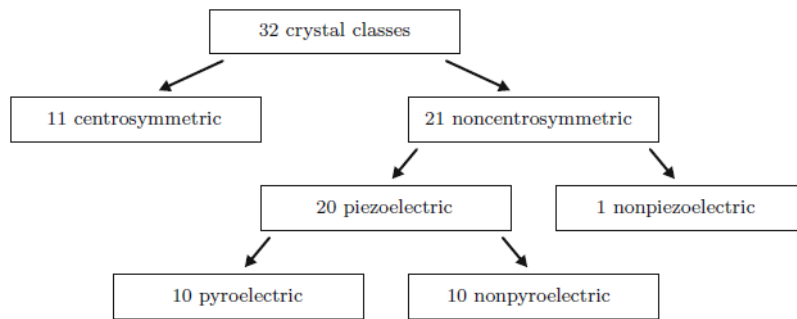


Figure 1.3: Classification of crystals

There are numerous materials, both natural and man-made, that exhibit various piezoelectric effects. Some naturally occurring piezoelectric materials include Berlinitite, cane sugar, quartz, Rochelle salt, topaz, tourmaline, and bone. Examples of man-made piezoelectric materials include barium titanate (BTO) and lead zirconate titanate (PZT) [13].

The choice of the piezoelectric material used to build piezoelectric sensors and actuators depends on the specific applications. A wide variety of applications require piezoelectric materials that are free from hysteresis behavior (discussed in section 1.3) and offer high mechanical stiffness. On the other hand, there are applications that necessitate mechanically flexible materials with piezoelectric properties. Therefore, finding a single piezoelectric material that is most suitable for all types of piezoelectric sensors and actuators is impossible.

1.2 Piezoelectric Actuators

An actuator is a generic term referring to devices that convert input energy into mechanical energy. Various actuators have been developed and put to practical use based on different types of input energy. The piezoelectric actuator is a device that utilizes the inverse piezoelectric effect. It achieves displacement by directly applying deformation to a solid, featuring higher displacement accuracy, larger generation force, and quicker response speed than other types of actuators. Although the magnitudes of piezoelectric voltages, movements, or forces are small and often require amplification, piezoelectric materials have been adapted to an impressive range of applications that demand only small amounts of displacement, typically less than a few thousandths of micro-meters.

The configuration of the piezoelectric actuator can vary significantly based on the application. They are particularly used for positioning, controlling vibration, and quick switching applications [5] [14].

1.2.1 Types of piezoelectric actuators

Piezo Stack Actuators

When multiple piezo elements are arranged on top of each other, it is referred to as a piezo stack actuator. This configuration is utilized to provide a low stroke with high blocking energy. Depending on your design requirements, this type of actuator can be either discrete or co-fired. In the case of a discrete configuration, complex structures are designed by using discs or by individually stacking completed piezoelectric ceramic rings and metal electrode foil through an adhesive. The typical operating voltage for discrete piezo stack actuators ranges from 500V to 1,000V. On the other hand, if the actuators are co-fired stack actuators, they are also known as monolithic stacks, and they do not use adhesives. Instead, they employ high-temperature sintering of the ceramic pile and complete electrode. The operating voltage for co-fired stack actuators can be as low as 200 volts. Regardless of whether they are co-fired or discrete, it is possible to protectively insulate these actuators from mechanical stresses and environmental impacts. Achieving this typically involves coating materials, leaving stacks bare, or enclosing them

within stainless steel.

Bending Actuators

The bending actuator generates a significant mechanical deflection in response to an electrical signal. Consequently, this deflection yields a large stroke with minimal blocking force compared to a stack actuator. A bending actuator employs two thin layers of piezoelectric ceramic bonded together, typically aligned in the direction of coinciding polarization with an electrically parallel connection. Upon applying an electrical input, one ceramic layer contracts while the other expands, inducing flexion in the actuator (see Figure 1.4). This type of actuator is the one utilized in the studies conducted in this thesis. Chapter 4.1 provides a depiction of the actuator used for the tests.

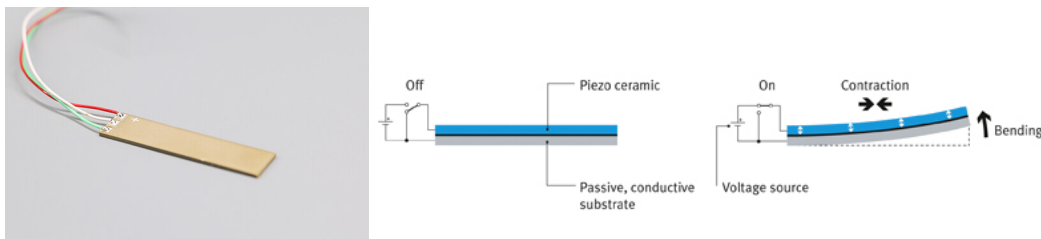


Figure 1.4: Bending actuator [1]

Longitudinal Actuators

Longitudinal actuators, also referred to as piezoelectric stacks, are created by layering multiple piezoelectric elements on top of each other. This arrangement ensures that the expansion effect of each element contributes to generating a useful force and movement (see Figure 1.5). These actuators leverage the piezoelectric effect to produce linear displacements ranging from 0.1% to 0.15% of the length of the actuator. Notably, these actuators exhibit a high force density, typically in the range of 30 N/mm^2 , and possess high resonant frequencies. As a result, longitudinal actuators are well-suited for dynamic applications.



Figure 1.5: Longitudinal actuator [2]

Shear Actuators

These types of actuators are akin to longitudinal actuators as they also consist of multiple layers of piezoelectric elements. However, they differ in the application of voltage and the type of motion they generate. In shear piezoelectric actuators, the individual elements are horizontally polarized, and the electrical field can be applied orthogonally. This configuration leads to a displacement occurring within the horizontal plane, resulting in a shear-type motion. Despite being limited in height due to bending and shear stresses, these actuators are often integrated into multi-axis systems alongside longitudinal actuators. This combination allows for a broader range of motion and functionality in various applications.

Tube Actuators

Tube actuators feature radial polarization and employ the transverse piezoelectric effect to induce displacement. These actuators can undergo radial, axial, or lateral motion depending on the applied voltage relative to the electrodes (see Figure 1.6). While these actuators are not suitable for generating substantial forces, they excel in providing micron-level travel. This makes them well-suited for applications such as pumping, nano-liter dosing, and scanning microscopes, where precise and fine-scale movements are crucial.

Contracting Actuators

Flat actuators, comprising two piezoelectric elements, can produce a con-



Figure 1.6: Tube actuator [3]

tracting motion when both elements operate concurrently. These actuators leverage the transverse piezoelectric effect to generate motion in a single direction. Contracting piezoelectric actuators exhibit limited displacement, up to 20 microns, but they can generate substantial force, often in the range of hundreds of Newtons. When this type of actuator is affixed to a substrate or base, it can be transformed into a bending actuator. In a bending-type actuator, the applied voltage can induce expansion in one piezoelectric element while the other contracts. This differential motion results in bending, allowing for controlled and precise movements in various applications.

1.2.2 Applications for piezoelectric actuators

Given its simple design, minimal moving parts, no requirement for lubrication to operate, and high reliability characteristics, the piezoelectric actuator is used in a variety of industrial, automotive, medical, aviation, aerospace, and consumer electronics applications. Piezoelectric actuators are found in precision knitting machinery and braille machines. The silent drive characteristics make piezoelectric actuators an excellent auto-focusing mechanism in microphone-equipped video cameras and mobile phones. Finally, since piezoelectric actuators require no lubrication to operate, they are used in cryogenic and vacuum environments. Using a stack actuator, extremely fine, virtually infinite resolution is possible with very high voltages corresponding to minute movements of expansion. A piezoelectric actuator can operate billions of times without wear or deterioration. Its response speed is exceptional

and is limited only by the inertia of the object being moved and the output capability of the electronic driver. When operating in an energized state, a piezoelectric actuator consumes virtually no power and generates very little heat [15].

Application examples in aerospace:

- **Micro-thrusters in satellites**, due to the high accuracy of piezoelectric actuators, they have found use in providing precise movement of micro thrusters in satellites (Figure 1.7) [16].

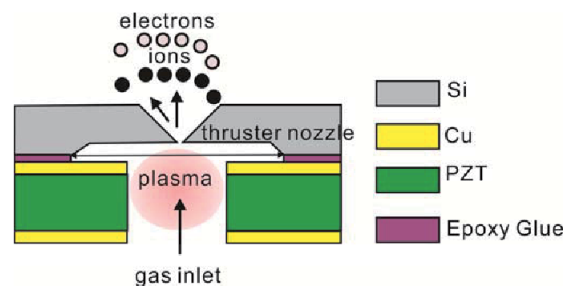


Figure 1.7: Piezoelectric micro-thruster

- **Active vibration damping**, piezoelectric actuators, when appropriately placed in a structure, can actively dampen noise. Noise and vibration reduction contribute to lowering the energy consumption of the craft [17].
- **Structural health monitoring**, the use of piezoelectric actuators allows for continuous monitoring of a structure's integrity. In transport, infrastructure, and building structures that require high levels of safety, continuous monitoring of structural health becomes highly relevant [18].

Application examples in medical field:

- **Nanopositioning**, the extremely precise nature of piezoelectric actuators makes positioning medical devices much more accurate. This increase in accuracy allows medical practitioners to more effectively perform treatments that require high accuracy such as surgery that

uses electro-mechanical devices that cut, position, and adjust parts within the body [19].

- **Laser position control**, in laser eye surgery a piezoelectric actuator controls the position of the laser used to perform the operation. Below is shown an image of a laser eye surgery which uses piezoelectric actuators to precisely position then move the laser pointed at one's eye. Accuracy in this situation is important because these procedures require the following of extremely exact paths [20].

Application examples in industry:

- **Piezoelectric gripper**, this application involves the use of a piezoelectric actuator to create a gripper capable of high force, quick response time, and nanometer precision (Figure 1.8) [21].

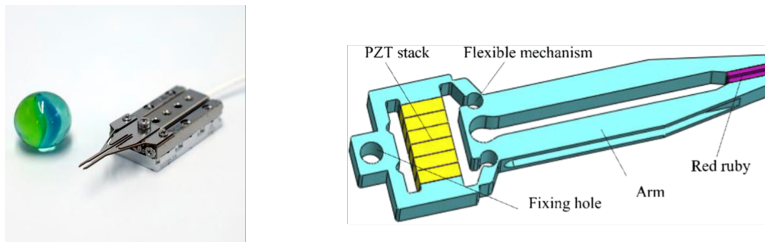


Figure 1.8: Piezoelectric gripper

- **Micro-machining**, similar to how piezoelectric actuators are used in larger scale industrial machining, micro-machining requires high precision. Given that piezoelectric actuators have precision down to the sub-nanometer scale and have high reliability, their use in the micro-machining process makes them invaluable for producing high-tolerance small scale parts. This value is because of the nanopositioning possible with these actuators and the need for nanopositioning in micro-machining [22].
- **Micro-assembly**, regardless of the end effector or tool used, the assembly of components at the nanometer/micrometer scale presents various challenges in terms of placement and joining. One way piezoelectric

actuators assist in addressing these challenges is through the precision and repeatability of their actuation. Micro assembly employs various methods that would be impossible without accurate positioning at the nanoscale. These methods include "pick and place" and guided transfer (Figure 1.9) [23].

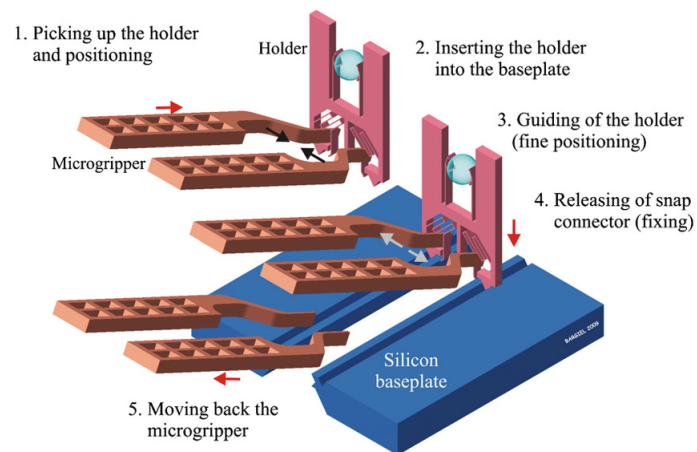


Figure 1.9: Piezoelectric micro-assembly example

- **Micro-pumping**, micropumps are simply pumps which function to move very small quantities of fluids at a time (Figure 1.10). The various constructions of micropumps include many varieties which involve the expansion and constriction of a space, a situation which lends itself to synergy with the shape changing nature of piezoelectric actuators [24].

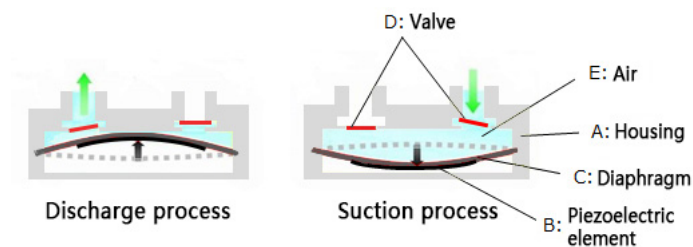
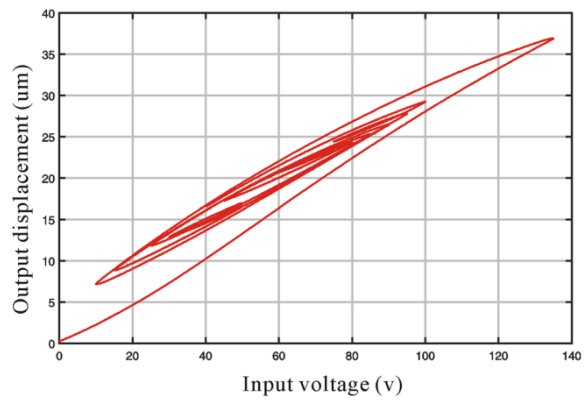


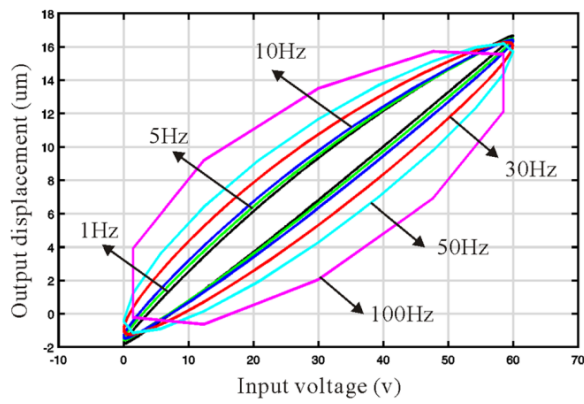
Figure 1.10: Piezoelectric micro-pump

1.3 Nonlinear behaviour: Hysteresis

A disadvantage of piezoelectric materials is its highly nonlinear input/output behavior. Specifically, a piezoelectric actuator shows hysteresis behavior, which affect their performance. In simple terms, this means that for a certain input, there is no unique output. Instead, the output depends on the input history. The term "hysteresis," derived from the Greek words meaning "deficiency" or "lagging behind," is defined as a dynamic lag phenomenon between the input voltage and output displacement or force of the piezoelectric actuator in the time domain operation. The lag size depends on the field level, cycle time, and materials used. It is often specified as a percentage of the total deflection achieved, ranging from 1% to 10%. The hysteresis characteristic of the piezoelectric actuator becomes noticeable when operating in a large voltage range with slow or fast speed motion, leading to significant positioning errors. Hysteresis occurs in both static and dynamic operations. Hysteresis behavior can be classified into rate-independent and rate-dependent hysteresis. Rate-independent hysteresis focuses on the relationships between input voltage and output displacement at low frequencies, while rate-dependent hysteresis considers the relationships between input voltage, input frequency (or rate), and output displacement. In Figure 1.11a, the existence of a hysteresis loop is clear, showing that the input voltage is not linear with the output displacement. In Figure 1.11b, hysteresis at different frequencies is depicted, illustrating how the lag increases as the frequency grows. Therefore, it is necessary to model the hysteresis behavior (see Chapter 2) and compensate for the hysteresis nonlinearity using control approaches (see Chapter 3) [25].



(a) Rate-independent behaviour



(b) Rate-dependent behaviour

Figure 1.11: Hysteresis curve

Chapter 2

Modelling of Piezoelectric Actuator

The objective of this chapter is to present which models are used in this thesis to study the piezoelectric actuator behaviour and the parameters identification.

Several models exist to represent the nonlinear behavior of the piezoelectric actuator, particularly due to hysteresis. Examples include the Preisach, Prandtl-Ishlinskii, Krasonsel'skii-Pokrovskii, Maxwell, Bouc-Wen, Duhem, Dahl, Linear, and Hysteron models [25][26]. In this thesis, the models considered are the Bouc-Wen model and a Port-Hamiltonian System (PHS) model based on hysterons. The piezoelectric actuator system model comprises two subsystems: electrical and mechanical. The electrical subsystem represents the hysteretic system, which is modeled differently based on the chosen model method (Bouc-Wen or PH). However, the mechanical subsystem is modeled as a mass-spring-damper system for both methods (Figure 2.1).

2.1 Bouc-Wen model

The Bouc–Wen model of hysteresis, introduced by Robert Bouc and extended by Yi-Kwei Wen, is a hysteretic model commonly used to describe nonlinear hysteretic systems [27]. This model, known for its simplicity and versatility, is capable of representing a wide class of hysteretic systems in analytical form.

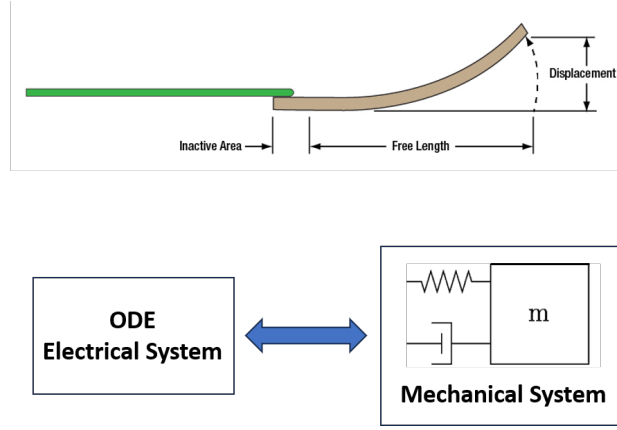


Figure 2.1: Piezoelectric Actuator Model

It is based on a state variable h and the relationship between a mechanical excitation F and the state h is given by the following differential equation:

$$\dot{h} = A\dot{F} - \beta \left| \dot{F} \right| h |h|^{n-1} - \gamma \dot{F} |h|^n \quad (2.1)$$

where A controls the restoring force amplitude, β and γ control the shape of the hysteresis loop and n controls the smoothness of the transition from elastic to plastic response. For different values of parameters β and γ , the hysteretic characteristics of the structure will change in different forms (Figure 2.2). When $\beta + \gamma > 0$ the structure presents soft characteristics, and the hysteretic restoring force of the system decreases as the displacement response increases. When $\beta + \gamma = 0$, the structure is linear in the loading stage. When $\beta + \gamma < 0$, the structure shows hardening properties, and the hysteretic restoring force of the system increases with the increase in displacement response [28].

Considering that in this thesis we work with a bending piezoelectric actuator, it is possible to consider $n = 1$. Adding the mass-spring-damper dynamics and replacing the mechanical input F with the applied input voltage V_{in} we obtain the following set of ordinary differential equations:

$$\begin{aligned} \dot{h} &= AV_{in} - \beta \left| \dot{V}_{in} \right| h - \gamma \dot{V}_{in} |h| \\ \dot{y} &= \frac{p}{M} \\ \dot{p} &= -ky - b\frac{p}{M} + K_v V_{in} - K_h h - F_{ext} \end{aligned} \quad (2.2)$$

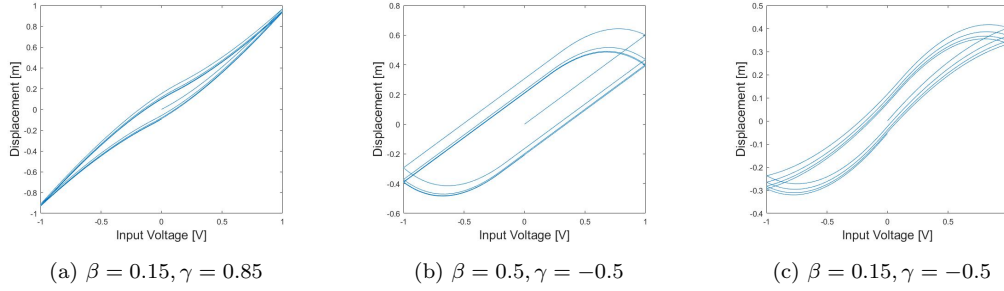


Figure 2.2: Bouc-Wen Hysteresis

where p is the mechanical momentum of PA, M is the mass of PA, k is the elastic stiffness of the model spring, b is the damping of the model damper and F_{ext} is the external force applied (considered equal to zero).

A simpler version of Bouc-Wen model exists, where the mechanical subsystem is represented by a gain d_p [29]. Now, the system equations is:

$$\begin{aligned} y(t) &= d_p V_{in}(t) - h(t) \\ \dot{h} &= A \dot{V}_{in} - \beta \left| \dot{V}_{in} \right| h - \gamma \dot{V}_{in} |h| \end{aligned} \quad (2.3)$$

where y is the final displacement of the piezoelectric actuator.

2.2 PHS model

The PHS model, which is based on hysterons, is based on the port-Hamiltonian system [9]. The considered Port-Hamiltonian system belongs to the class of affine input mapping.

Definition 2.2.1. An input affine PHS is defined in a state space $x \in \mathbb{R}^n$ as the following system:

$$\Sigma = \begin{cases} \dot{x} = [J(x) - D(x)] \frac{\partial H}{\partial x} + g(x)u \\ y = g(x)^T \frac{\partial H}{\partial x} \end{cases} \quad (2.4)$$

where $H : \mathbb{R}^n \rightarrow \mathbb{R}$ is the Hamiltonian function, $J(x) \in \mathbb{R}^{n \times n}$ is a skew-symmetric interconnection matrix, $D(x) \geq 0, D(x) = D(x)^T \in \mathbb{R}^{n \times n}$ is a positive semi-definite dissipation matrix, $u \in \mathbb{R}^m$ is the input vector and $g(x) \in \mathbb{R}^{n \times m}$ is the input mapping.

The Hamiltonian function H , called also the energy function, represents the total energy of a system.

The considered dynamic system equations represented by a PHS model, taken from [4], are:

$$\begin{aligned} \dot{q} &= \frac{p}{M} \\ \dot{p} &= -\alpha \sum_{i=1}^n \frac{Q_i}{C_i} - kq - b\frac{p}{M} + \alpha V_{in} - F_{ext} \\ \dot{Q}_i &= -h_i^{-1}\left(\frac{Q_i}{C_i}\right) + \alpha \frac{p}{M} \quad i = 1 \dots n \end{aligned} \quad (2.5)$$

where q is the displacement, p is the mechanical momentum and M the mass of the piezoelectric actuator. The k and b are respectively the elastic stiffness and the damping factor of the mechanical model. The α is the model transducer ratio, Q_i and C_i are the charge and the capacitance of the i th hysteron. V_{in} is the input voltage and F_{ext} is the external force applied (that will be considered equal to zero). $-h_i^{-1}$ is the nonlinear damping on the i th hysteron (Figure 2.3), its equation is:

$$h_i^{-1} = \begin{cases} \rho_i\left(\frac{Q_i}{C_i} + \frac{d_i}{2}\right) & \text{if } \frac{Q_i}{C_i} < -\frac{d_i}{2} \\ 0 & \text{if } -\frac{d_i}{2} \leq \frac{Q_i}{C_i} \leq \frac{d_i}{2} \\ \rho_i\left(\frac{Q_i}{C_i} - \frac{d_i}{2}\right) & \text{if } \frac{Q_i}{C_i} > \frac{d_i}{2} \end{cases} \quad (2.6)$$

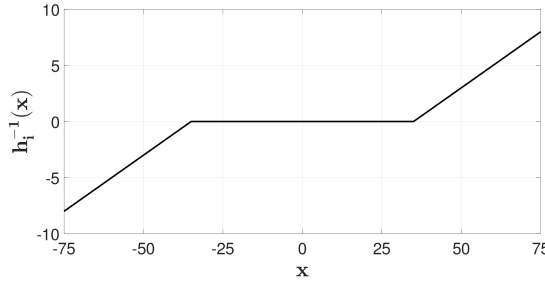


Figure 2.3: Nonlinear damping example

Moreover the following proposition holds [4]:

Proposition 2.2.1. *The system described by (2.5) is a PHS (2.4) with state vector the energy variables of the system $x = [Q_i \ \dots \ q \ p]^T$, Hamiltonian function the electro-mechanical energy of the system*

$$H(x) = \frac{1}{2}x^T \mathcal{H}x \quad (2.7)$$

where $\mathcal{H} = \text{diag}([1/C_i \ \dots \ k \ 1/m])$, the input vector is $u = [V_{in} \ F_{ext}]^T$ and the system matrices are

$$\begin{aligned}
 J &= \begin{bmatrix} 0 & \dots & 0 & \alpha \\ \vdots & \ddots & \vdots & \vdots \\ 0 & \dots & 0 & 1 \\ -\alpha & \dots & -1 & 0 \end{bmatrix} & D(x) &= \begin{bmatrix} h_i^{-1}(\frac{Q_i}{C_i})\frac{C_i}{Q_i} & \dots & 0 & 0 \\ \vdots & \ddots & \vdots & \vdots \\ 0 & \dots & 0 & 0 \\ 0 & \dots & 0 & b \end{bmatrix} \\
 g &= \begin{bmatrix} 0 & 0 \\ \vdots & \vdots \\ 0 & 0 \\ \alpha & -1 \end{bmatrix}
 \end{aligned} \tag{2.8}$$

Furthermore, the forced equilibrium point

$$x^* = \begin{bmatrix} Q_1^* \\ \vdots \\ Q_n^* \\ \frac{\alpha}{k}(V_{in} - \sum_{i=1}^n \frac{Q_i^*}{C_i}) - \frac{1}{k}F_{ext} \end{bmatrix} \tag{2.9}$$

where $h_i^{-1}(Q_i^*/C_i) = 0$, is globally asymptotically stable.

See [4] for the proof.

2.3 Model Identification

The models identifications process is presented in [4]. For the PHS model the mass M is obtained by weighting the piezoelectric actuator used in the experiments for this thesis and the others mechanical parameters k and b are estimated from the step train response.

Subsequently, for the PHS model (2.5), the *'tfest'* function of MATLAB is utilized to find the transfer function, and it is possible to notice that a minimum of 2 hysteron are needed to represent the step response ($n = 2$). The electrical parameters are then estimated from that transfer function to serve as the initial point for a linear grey-box estimation. This linear estimation is carried out using the *'greyest'* function of MATLAB. The nonlinear parameters are obtained by employing the *'nlgreyest'* function with the *'lsqnonlin'*

Parameter	Value	Unit
M	$1.0148 \cdot 10^{-3}$	$[kg]$
k	24579	$[N/m]$
b	3.7356	$[Ns/m]$
C_1	$5.6425 \cdot 10^{-7}$	$[F]$
C_2	$5.2125 \cdot 10^{-7}$	$[F]$
α	0.046311	$[C/m]$
ρ_1^{-1}	0.6002	$[\Omega^{-1}]$
ρ_2^{-1}	$1.1528 \cdot 10^{-4}$	$[\Omega^{-1}]$
d_1	14.5126	$[V]$
d_2	8.6838	$[V]$

Table 2.1: PHS model parameters

method from the '*Optimization Toolbox*' in MATLAB. The parameter values found are presented in Table 2.1.

For the Bouc-Wen model (2.2) parameters the '*nlgreyest*' function of MatLab is used. The parameters values found are showed in Table 2.2.

In the model comparison reported in [4], it is demonstrated that for sinusoidal inputs within a frequency range of 1-150 Hz, both models exhibit a good fit percentage consistently exceeding 90%. Notably, for the Bouc-Wen model, the fit percentage decreases as the frequency increases, while the PHS model's fit percentage remains mostly constant, exceeding 96.5%. The step input was not included in the comparison, as the vibration and creep were not modeled in the two hysteron model and could compromise the sinusoidal response. The plots (Figures 2.4, 2.5, and 2.6), as well as the table values (Table 2.3), extracted from [4], illustrate the considerations outlined above.

Parameter	Value	Unit
M	$9.4023 \cdot 10^{-4}$	$[kg]$
b	5.2	$[Ns/m]$
k	24579	$[N/m]$
A	0.008743	$[V^{-1}]$
β	0.00637	$[V^{-1}]$
γ	0.0144905	$[V^{-1}]$
K_v	0.048676	$[N/V]$
K_h	1.9767	$[N]$

Table 2.2: Bouc-Wen model parameters

Experiments	PHS	Bouc-Wen
$1Hz$	97.11	96.35
$10Hz$	97.23	94.97
$25Hz$	97.41	94.02
$50Hz$	96.59	93.06
$75Hz$	96.69	91.75
$100Hz$	96.99	90.80
$150Hz$	96.98	90.14

Table 2.3: Models fit percentages (%)

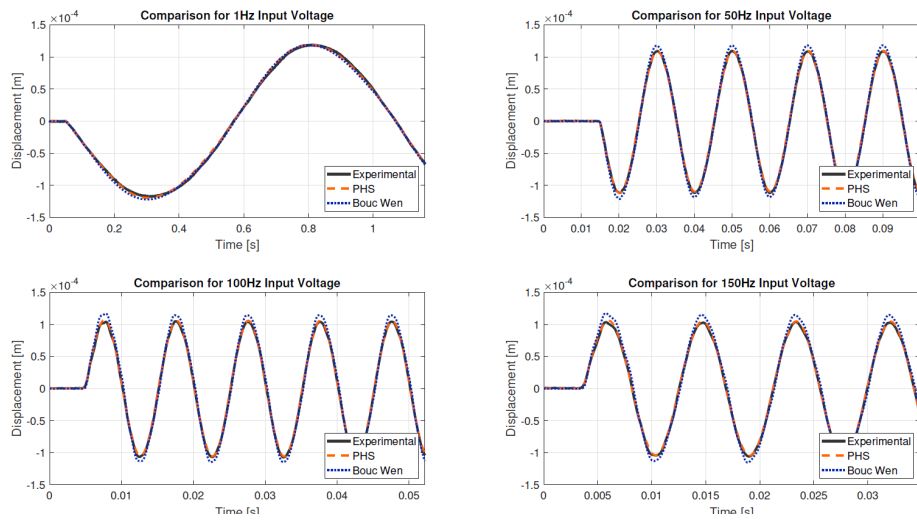


Figure 2.4: Sinusoidal input response

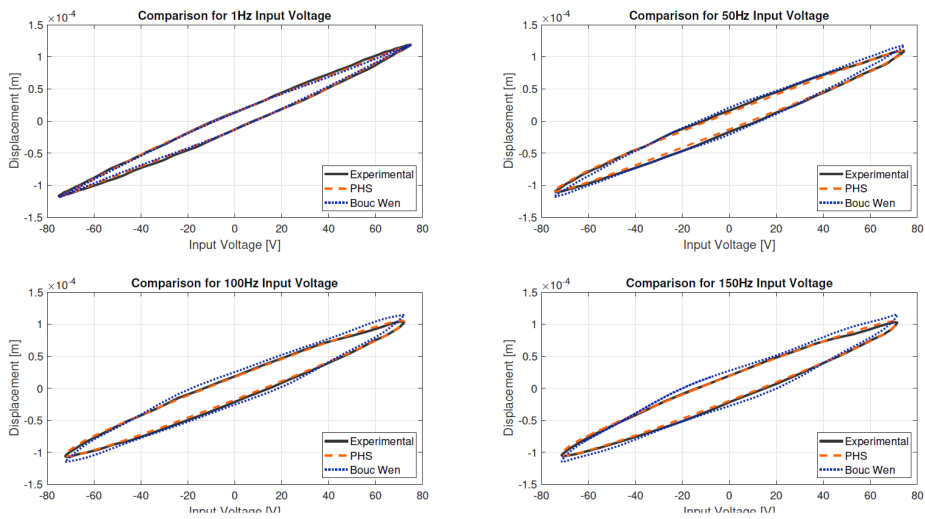


Figure 2.5: Hysteresis for sinusoidal input

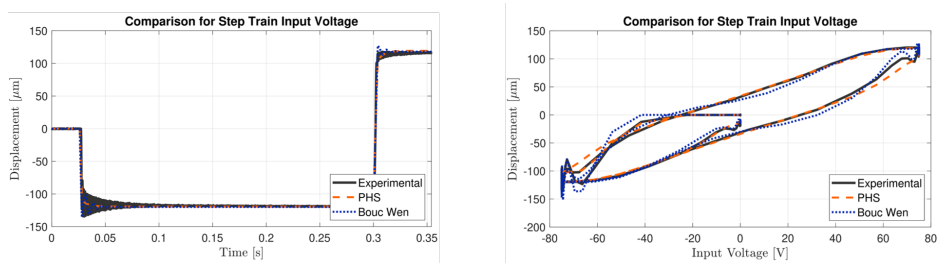


Figure 2.6: Step input response

Chapter 3

PI Control

The objective of this chapter is to present a practical approach to finding the gains of the PI controller through model simplification using the pole placement method. Two designs for PI controllers are proposed: one considering the PHS model, with identification based on sinusoidal response, and the other considering a new identification based on the step response. The corresponding PHS parameters for the new identification are determined. Simulations on Simulink are conducted for both PI controllers. Finally, a global stability analysis is carried out.

3.1 Controller Design

The chosen control type is a Proportional-Integral (PI) controller (Figure 3.1), which aids in reducing both the rise time and the steady-state errors of the system [7].

$$u(t) = K_p e(t) + K_i \int e(t) \quad (3.1)$$

where $e(t)$ is the error, defined as the difference between the reference signal and the output signal. In our case, the reference is considered as the desired position, and the output signal is the actual displacement of the piezoelectric actuator.

The proposed strategy for designing the PI controller involves using a pole placement approach to find the values for K_p and K_i that meet the requirements of no overshoot and no oscillations. Since we are dealing with the

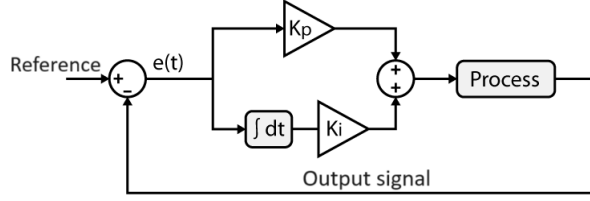


Figure 3.1: PI controller block diagram

PHS model, a nonlinear model (3.2), the idea is to obtain a simplified model through linearization and order reduction from 4th to 2nd order. This allows us to leverage the extensive literature available for 2nd order systems.

$$\begin{aligned}
 \dot{q} &= \frac{p}{M} \\
 \dot{p} &= -\alpha\left(\frac{Q_1}{C_1} + \frac{Q_2}{C_2}\right) - kq - b\frac{p}{M} + \alpha V_{in} \\
 \dot{Q}_1 &= -h_1^{-1}\left(\frac{Q_1}{C_1}\right) + \alpha\frac{p}{M} \\
 \dot{Q}_2 &= -h_2^{-1}\left(\frac{Q_2}{C_2}\right) + \alpha\frac{p}{M}
 \end{aligned} \tag{3.2}$$

The analysis is made through the following steps:

- **step 1)** Choose the dynamic model, we use the PHS model showed above, as demonstrated in Chapter 2.3, it performs better than Bouc-Wen model;
- **step 2)** Linearize the model, we still have a 4th order model;
- **step 3)** Reduce the order model from 4th to 2nd. Assuming that the main contribution to the dynamics is given by the mechanical subsystem, we can neglect the electrical subsystem dynamics;
- **step 4)** Apply the pole placement method.

Since we have already chosen the model, we move on to the second step: the linearization of the model. The model is nonlinear due to h_1^{-1} and h_2^{-1} that are not linear functions (Figure 2.3):

$$h_i^{-1} = \begin{cases} \rho_i\left(\frac{Q_i}{C_i} + \frac{d_i}{2}\right) & \text{if } \frac{Q_i}{C_i} < -\frac{d_i}{2} \\ 0 & \text{if } -\frac{d_i}{2} \leq \frac{Q_i}{C_i} \leq \frac{d_i}{2}, \quad i = 1, 2 \\ \rho_i\left(\frac{Q_i}{C_i} - \frac{d_i}{2}\right) & \text{if } \frac{Q_i}{C_i} > \frac{d_i}{2} \end{cases} \tag{3.3}$$

The linearization is performed by neglecting the dead zone. Therefore, the linearized expression for h_i^{-1} is:

$$\tilde{h}_i^{-1} = \rho_i \frac{Q_i}{C_i}, \quad i = 1, 2 \quad (3.4)$$

Consequently, the linearized dynamic system equations is:

$$\begin{aligned} \dot{\tilde{q}} &= \frac{p}{M} \\ \dot{\tilde{p}} &= -\alpha \left(\frac{Q_1}{C_1} + \frac{Q_2}{C_2} \right) - kq - b \frac{p}{M} + \alpha V_{in} \\ \dot{\tilde{Q}}_1 &= -\rho_1 \frac{Q_1}{C_1} + \alpha \frac{p}{M} \\ \dot{\tilde{Q}}_2 &= -\rho_2^{-1} \frac{Q_2}{C_2} + \alpha \frac{p}{M} \end{aligned} \quad (3.5)$$

This results in a 4th-order linear system, where the mechanical subsystem is represented by the 1st and 2nd equations, and the electrical subsystem is represented by the 3rd and 4th equations. The third step is to reduce the model. Since the electrical part is faster than the mechanical one, the dynamics are mainly affected by the mechanical subsystem. It is allowed to consider the electrical contribution as instantaneous changes, which means that $\dot{\tilde{Q}}_1$ and $\dot{\tilde{Q}}_2$ are equal to zero:

$$\begin{aligned} \dot{\tilde{q}} &= \frac{p}{M} \\ \dot{\tilde{p}} &= -\alpha \left(\frac{Q_1}{C_1} + \frac{Q_2}{C_2} \right) - kq - b \frac{p}{M} + \alpha V_{in} \\ 0 &= -\rho_1 \frac{Q_1}{C_1} + \alpha \frac{p}{M} \\ 0 &= -\rho_2^{-1} \frac{Q_2}{C_2} + \alpha \frac{p}{M} \end{aligned} \quad (3.6)$$

Now, it is possible to obtain Q_1 and Q_2 from the 3th and 4th equations:

$$\begin{aligned} Q_1 &= \alpha \frac{p}{M} \frac{C_1}{\rho_1} \\ Q_2 &= \alpha \frac{p}{M} \frac{C_2}{\rho_2} \end{aligned} \quad (3.7)$$

substituting in the 2nd equation, the resultant final dynamic system equation is:

$$\begin{aligned} \dot{\tilde{q}} &= \frac{p}{M} \\ \dot{\tilde{p}} &= -\left[\frac{\alpha^2}{M} \left(\frac{1}{\rho_1} + \frac{1}{\rho_2} \right) + b \frac{p}{M} \right] - kq + \alpha V_{in} \end{aligned} \quad (3.8)$$

Now let's proceed with the fourth step, applying the pole placement method.

Following are presented the two PI controller designs. The first one is a continuation of the above analysis, where the PI controller is based on the 2nd order simplified system derived from the PHS model, which was identified by sinusoidal response. The second one is also based on a 2nd order system, with identification based on the step response.

3.1.1 PI based on sinusoidal response identified model

The first proposed PI controller is designed considering the system analyzed above, where its identification is based on the sinusoidal response (see Chapter 2.3). Substituting the parameters from Table 2.1 into the system 3.8, the corresponding transfer function is:

$$\frac{45.64}{s^2 + 22017s + 2.422 \cdot 10^7} \quad (3.9)$$

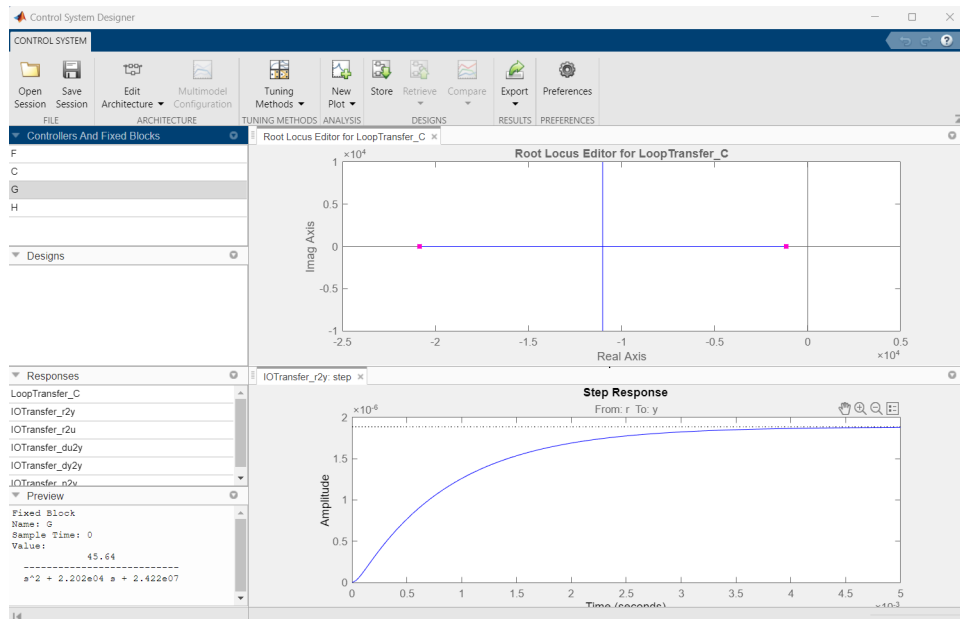


Figure 3.2: Control System Designer

As show in Figure 3.2 the poles of the open loop system are:

$$\begin{aligned} p_1 &= -2.0716 \cdot 10^4 \\ p_2 &= -0.1169 \cdot 10^4 \end{aligned} \quad (3.10)$$

As a last step, once a simplified 2nd-order system is obtained, it becomes easier to find the gain values for the PI controller, K_p and K_i , by applying the pole placement approach. Using the '*Control System Designer Tool*' in MatLab, it is possible to analyze the closed-loop system with Output Step Response, Rootlocus, etc., and choose the desired type of control. This tool requires the transfer function of the system. To obtain a PI controller, we add an integrator and a real zero.

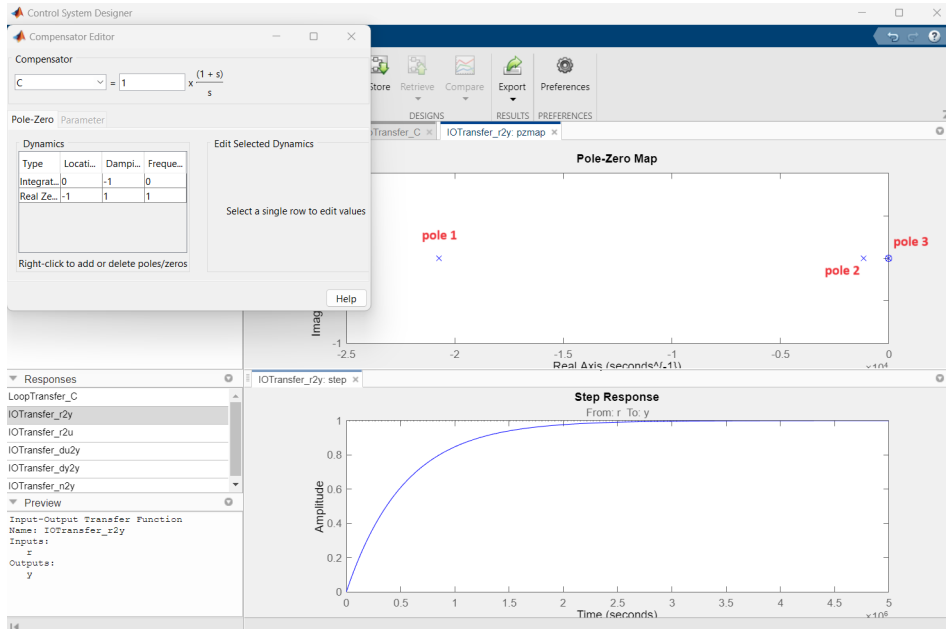


Figure 3.3: Control System Designer - PI controller

Once the PI controller is added (Figure 3.3), the new system is of order three, providing an additional degree of freedom (DOF) that allows us to choose the desired pole position. Considering:

$$\begin{aligned} u(t) &= K_p e(t) + K_i \int e(t) = K_p(r - q) + v \\ \dot{v} &= K_i e(t) = K_i(r - q) \end{aligned} \quad (3.11)$$

where $u(t) = V_{in}$, r is the reference signal and q is the output signal. Substituting, the controlled dynamics becomes:

$$\begin{aligned} \dot{\tilde{q}} &= \frac{p}{M} \\ \dot{p} &= -\left[\frac{\alpha^2}{M}\left(\frac{1}{\rho_1} + \frac{1}{\rho_2}\right) + b\frac{p}{M}\right]p - (k + \alpha K_p)q + \alpha K_p r + \alpha v \\ \dot{v} &= K_i(r - q) \end{aligned} \quad (3.12)$$

We would like to obtain a faster response time, but we have to be careful to avoid overshooting, which is mainly caused by conjugate poles. Having poles with negative real parts guarantees asymptotic stability. Consequently, the idea is to still have negative real poles and ensure a robust system, therefore working with a more reliable system.

Remember that if K_p increases the rise time decreases, and if K_i increases the steady state error decreases [7]. Moving pole 3 further away from real axis and making poles 1 and 2 closer helps to achieve the goal. Be careful to not move poles 1 and 2 too close; otherwise, we have overshooting. After some trials, we get a satisfying system behaviour with the following poles (Figure 3.4):

$$\begin{aligned} p_1 &= -1.8612 \cdot 10^4 \\ p_2 &= -0.2195 \cdot 10^4 \\ p_3 &= -0.1078 \cdot 10^4 \end{aligned} \quad (3.13)$$

In Figure (3.5), the root locus of the simplified system before and after PI controller is shown, *sys2* is the simplified system of 2nd order and *sys2C* is the same system with PI controller.

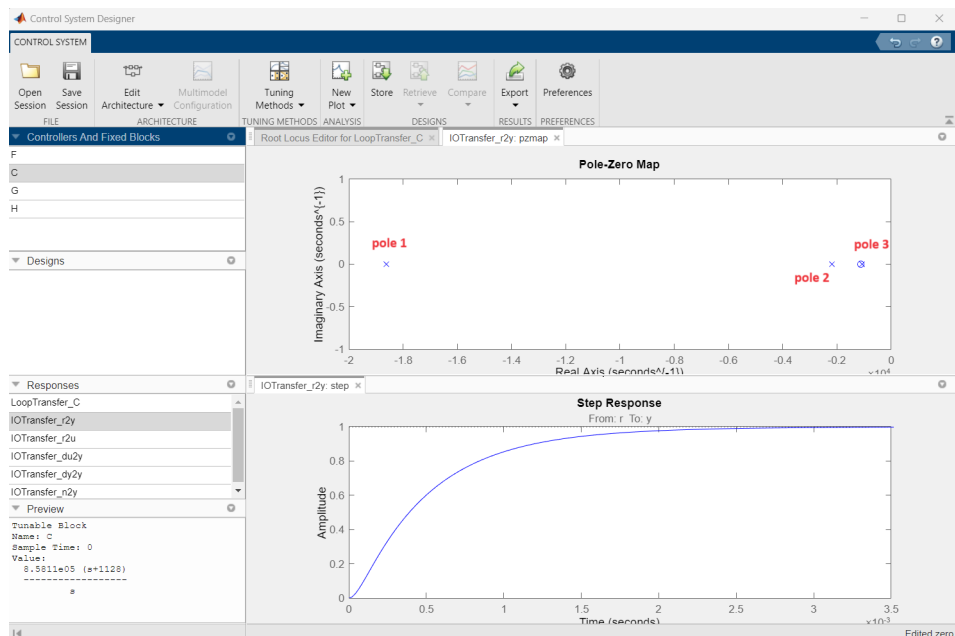


Figure 3.4: Control System Designer - Final system with PI controller

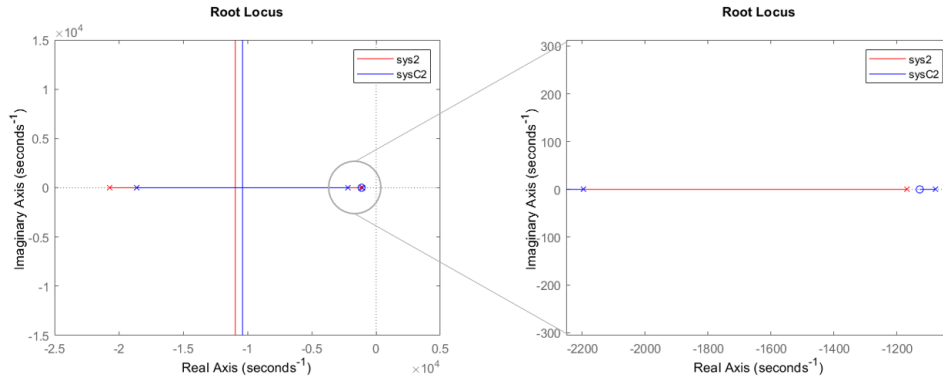


Figure 3.5: Root Locus comparison

The gain values founded are:

$$\begin{aligned} K_p &= 8.5811 \cdot 10^5 \\ K_i &= 9.6755 \cdot 10^8 \end{aligned} \quad (3.14)$$

3.1.2 PI based on step response identified model

Another PI controller design is proposed, it is based on a new identification model. The new model identification is carried out considering the step response, while the previous one was based on sinusoidal response. The model identified, through *'tfest'* Matlab function, is of 2nd order. In this way, we can apply the same procedure to design the PI controller. The transfer function obtained is:

$$\frac{16.78}{s^2 + 2555s + 9.539 \cdot 10^6} \quad (3.15)$$

The fit percentage is of 78.25%.

Once the new transfer function is obtained, it is possible to proceed with the design of the PI controller. Similar to the other model, we apply the pole placement method using the *'Control System Designer'* tool of MatLAB. In Figure 3.6 the poles of the open loop system are showed. Again, we create a PI controller by adding an integrator and a real zero. The consideration made previously to find K_p and K_i are still valid. However, in this case, we obtain the 2nd order transfer function directly from the identification of the real plant behaviour, not through a linearization and a simplification of

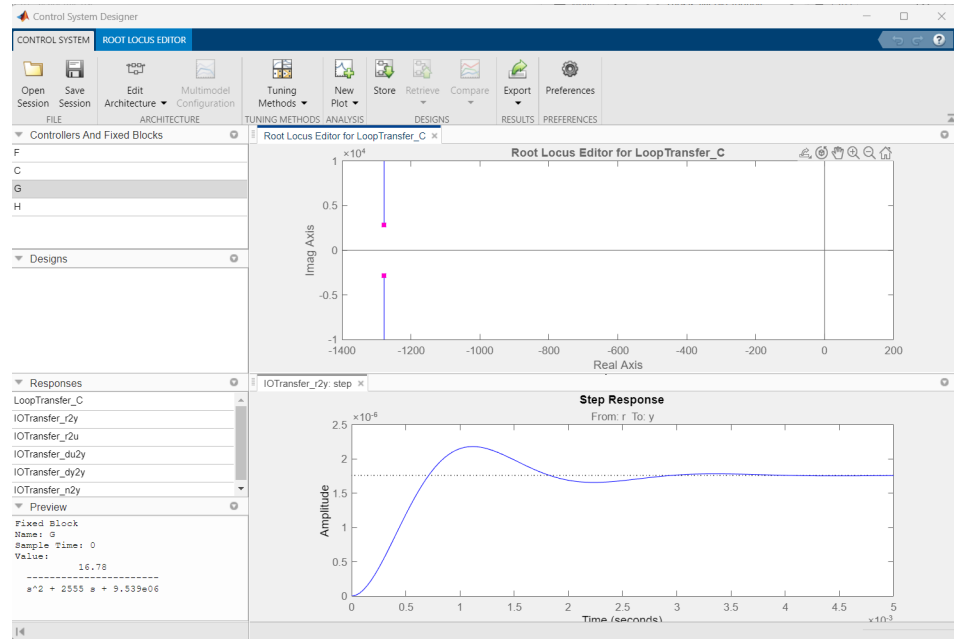


Figure 3.6: Control System Designer - Open loop system

another system. Therefore, we have a better representation of the real plant oscillations and we have to deal with complex conjugates poles to reduced the overshoot. Adjusting the new pole and zero, added due to the controller, it is possible to obtained an overdamped system.

The new K_p and K_i found are:

$$\begin{aligned} K_p &= 2.3164 \cdot 10^4 \\ K_i &= 1.8384 \cdot 10^8 \end{aligned} \quad (3.16)$$

3.1.3 Parameters comparison

To identify the parameters of the new model, we proceed with a comparison between the obtained transfer function (TF) and the one derived trough the PHS model simplification, expressed with parameters. Starting from system 3.8 we obtain the state space (SS) matrices A, B, C and D . Remember that

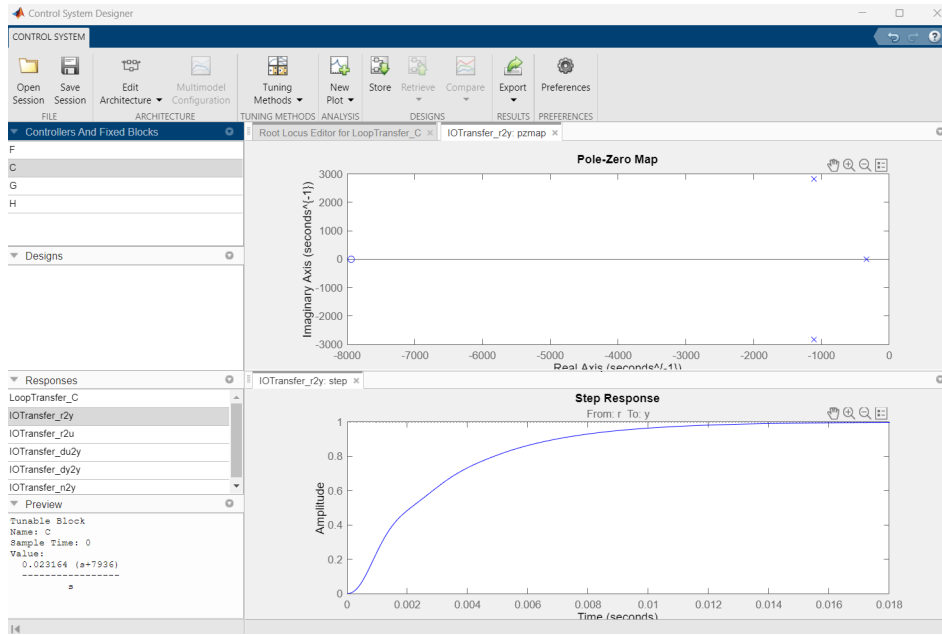


Figure 3.7: Control System Designer - Closed loop system

the output y is the displacement q .

$$\begin{aligned} A &= \begin{bmatrix} 0 & \frac{1}{M} \\ -k & -\beta \end{bmatrix} & B &= \begin{bmatrix} 0 \\ \alpha \end{bmatrix} \\ C &= \begin{bmatrix} 1 & 0 \end{bmatrix} & D &= [0] \end{aligned} \quad (3.17)$$

where β is $\frac{\alpha^2}{M}(\frac{1}{\rho_1} + \frac{1}{\rho_2}) + \frac{b}{M}$. Now, we express the transfer function with parameters. From SS to TF the equation is:

$$TF = \frac{CA \text{adj}(sI - A)B + D}{\det(sI - A)} \quad (3.18)$$

$$\begin{aligned} (sI - A) &= \begin{bmatrix} s & -\frac{1}{M} \\ k & s + \beta \end{bmatrix} \\ \text{adj}(sI - A) &= \begin{bmatrix} s + \beta & \frac{1}{M} \\ -k & s \end{bmatrix} \\ \det(sI - A) &= s^2 + \beta s + \frac{k}{M} \\ CA \text{adj}(sI - A)B + D &= \frac{\alpha}{M} \end{aligned} \quad (3.19)$$

Following the parameterized TF is:

$$TF = \frac{\frac{\alpha}{M}}{s^2 + \beta s + \frac{k}{M}} \quad (3.20)$$

Let's found now the parameters M, α, k, b, ρ_1 and ρ_2 for the new model identification (3.15). We have to much parameters and some assumptions are needed:

- the mass M is the same for both models, $M = 1.0148 \cdot 10^{-3}$;
- β is considered only equal to $\frac{b}{M}$;
- the parameters ρ_1 and ρ_2 are supposed equal.

To find α we consider the numerator $\frac{\alpha}{M}$ and the solution is streetforward

$$\alpha = 16.78 \cdot M = 0.017028 \quad (3.21)$$

The same procedure is done to find k considering the constant term of the denominator $\frac{k}{M}$, consequently

$$k = 9.539 \cdot 10^6 \cdot M = 9680.2 \quad (3.22)$$

For b , same approach considering the second assumption,

$$b = 2555 \cdot M = 2.5928 \quad (3.23)$$

While, to find $\rho(= \rho_1 = \rho_2)$ we consider the total β where α and b are the new values find above

$$\rho^{-1} = \frac{M\beta - b}{2\alpha^2} = 0.024 \quad (3.24)$$

In Table 3.1 it is possible to compare the previous parameters (for 2nd order PHS model) and the ones obtained above. The parameters are not too different, they have the same order of magnitude, so we have two comparable system. Only k differ of one order of magnitude, and since it is smaller, this just tell us that the new model is less elastic.

Let's analyse also the damping factor ζ , which depends on $\beta = \frac{\alpha^2}{M}(\frac{1}{\rho_1} + \frac{1}{\rho_2}) + \frac{b}{M}$. Considering the denominator of the TFs and knowing that we can be represented it in function of the damping factor ζ and the natural frequency ω_n [30]:

$$s^2 + \beta s + \frac{k}{M} = s^2 + 2\zeta\omega_n s + \omega_n^2, \quad (3.25)$$

consequently we can calculate $\zeta = \frac{\beta}{2\sqrt{k/M}}$.

Parameter	Value OLD	Value NEW	Unit
M	$1.0148 \cdot 10^{-3}$	$1.0148 \cdot 10^{-3}$	$[kg]$
k	24579	9680.2	$[N/m]$
b	3.7356	2.5928	$[Ns/m]$
α	0.046311	0.017028	$[C/m]$
ρ_1^{-1}	0.6002	0.024	$[\Omega^{-1}]$
ρ_2^{-1}	$1.1528 \cdot 10^{-4}$	0.024	$[\Omega^{-1}]$

Table 3.1: Model parameters comparison

For PHS simplified model (3.9), the damping factor is:

$$\zeta_{PHS} = \frac{22017}{2\sqrt{24579/1.0148 \cdot 10^{-3}}} = 2.24 \quad (3.26)$$

For the new identified model (3.15), the damping factor is:

$$\zeta = \frac{2555}{2\sqrt{9680.2/1.0148 \cdot 10^{-3}}} = 0.41 \quad (3.27)$$

As found in the open loop analysis, in the PI controllers design, the first system results over-damped ($\zeta > 1$) and the second one is under-damped ($\zeta < 1$) [30].

3.2 Simulations

In this section we want to simulate the controlled system. Firstly considering the 2nd order PHS simplified model (3.8) and the nonlinear PHS model (3.2), with the first PI controller found (3.14). Consequently, considering the new identification model (3.15), with the second PI controller (3.16). The simulations are made using the Simulink software of MatLab.

For the sake of simplicity the 2nd order simplified PHS linear system with PI controller will indicated as PHS_2 , the original 4th order PHS nonlinear system with PI controller as PHS_{NL} and the new identified 2nd order model with PI controller as $NewId_2$.

Following it is possible to see the plots, where the color legend is:

- **yellow** is the reference signal;

- **blue** is referred to PHS_{NL} ;
- **green** is referred to PHS_2 ;
- **orange** is referred to $NewId_2$.

The reference signals taking into account are a square wave signal and sine wave signal with frequencies of 1, 50, 100 and 150Hz, the amplitude for both signals is $120\mu m$.

How we expected, due to the controller design, the step response for PHS_2 is over-damped (Figure 3.9). For PHS_{NL} we have a similar behaviour but, of course, it is visible the nonlinear component and how firstly acts the K_p , that can't reach the position reference, and after there is the K_i contribution to arrive at steady state conditions (Figure 3.9). The idea to avoid overshoot is due to ensure that a too abruptly change not occurs when working near the maximum displacement for the piezoelectric actuator ($120\mu m$), otherwise it could brake. Considering that the PHS_{NL} behaviour follows this concept and it can be considered a good result.

Looking now to the sinusoidal response for PHS_2 it is clear how the PI controller works better at lower frequencies (Figure 3.10). From the hysteresis plots it is possible to notice that as well, increasing the frequencies increases the gap and it slowly turns clockwise (Figure 3.10). The sine wave plots and its hysteresis for PHS_{NL} (Figure 3.10) are very similar to the one of PHS_2 , this is good, it means that the PI controller found through simplifications it is valid for the nonlinear system.

About $NewId_2$, the step response (Figure 3.9) is slower compared to PHS models, but this is the compromise to have no overshoot and no oscillations. The sinusoidal response for $NewId_2$ (Figure 3.10) is taking into account a feedforward action. Without adding a feedforward control the response wasn't enough good to have comparable results.

Feedforward control is typically added to feedback control and it is a strategy to reject persistent disturbances that cannot adequately be rejected with only feedback [7]. We test, now, the new PI controller with sine wave input adding a feedforward action to better tracking the reference. Considering equation 3.28, with $V_{in}^* = \frac{k}{\alpha}r(t)$ (Figure 3.8).

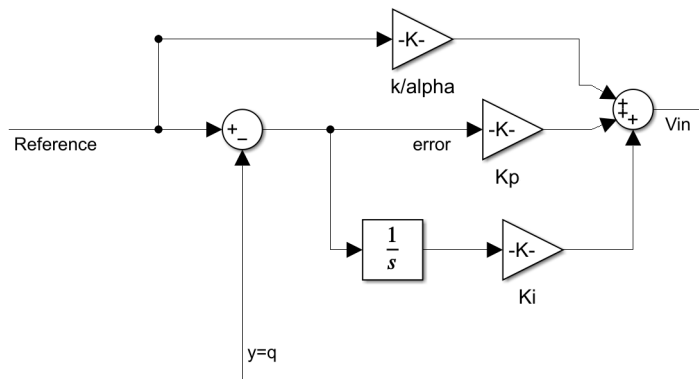


Figure 3.8: Feedforward action

As for the PHS models, the *NewId₂* sinusoidal response is behaving better at lower frequencies, clearly visible in the hysteresis plots (Figure 3.10). At higher frequencies the displacement overpasses the reference, actually this is not physically possible since $120\mu\text{m}$ is the maximum displacement. However, *NewId₂* is identified based on step response with considering the sinusoidal response, therefore we don't expect a correct behaviour.

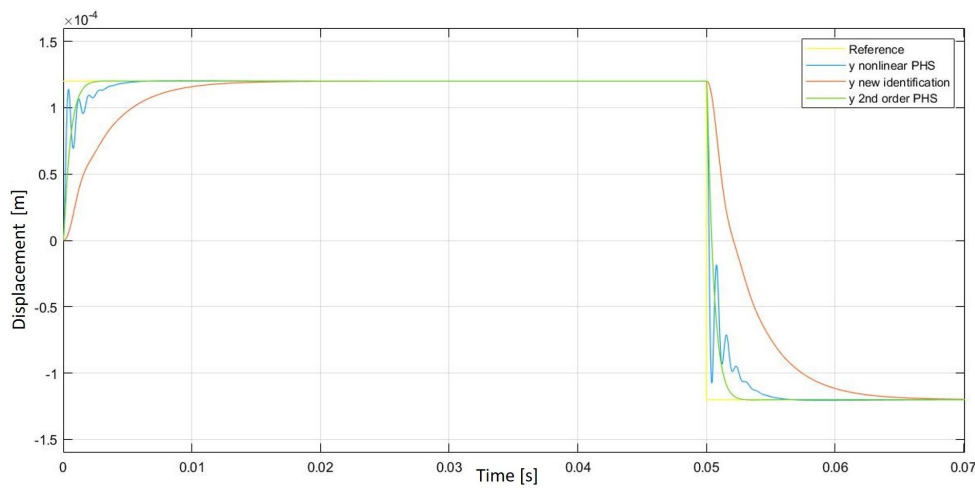


Figure 3.9: Step response

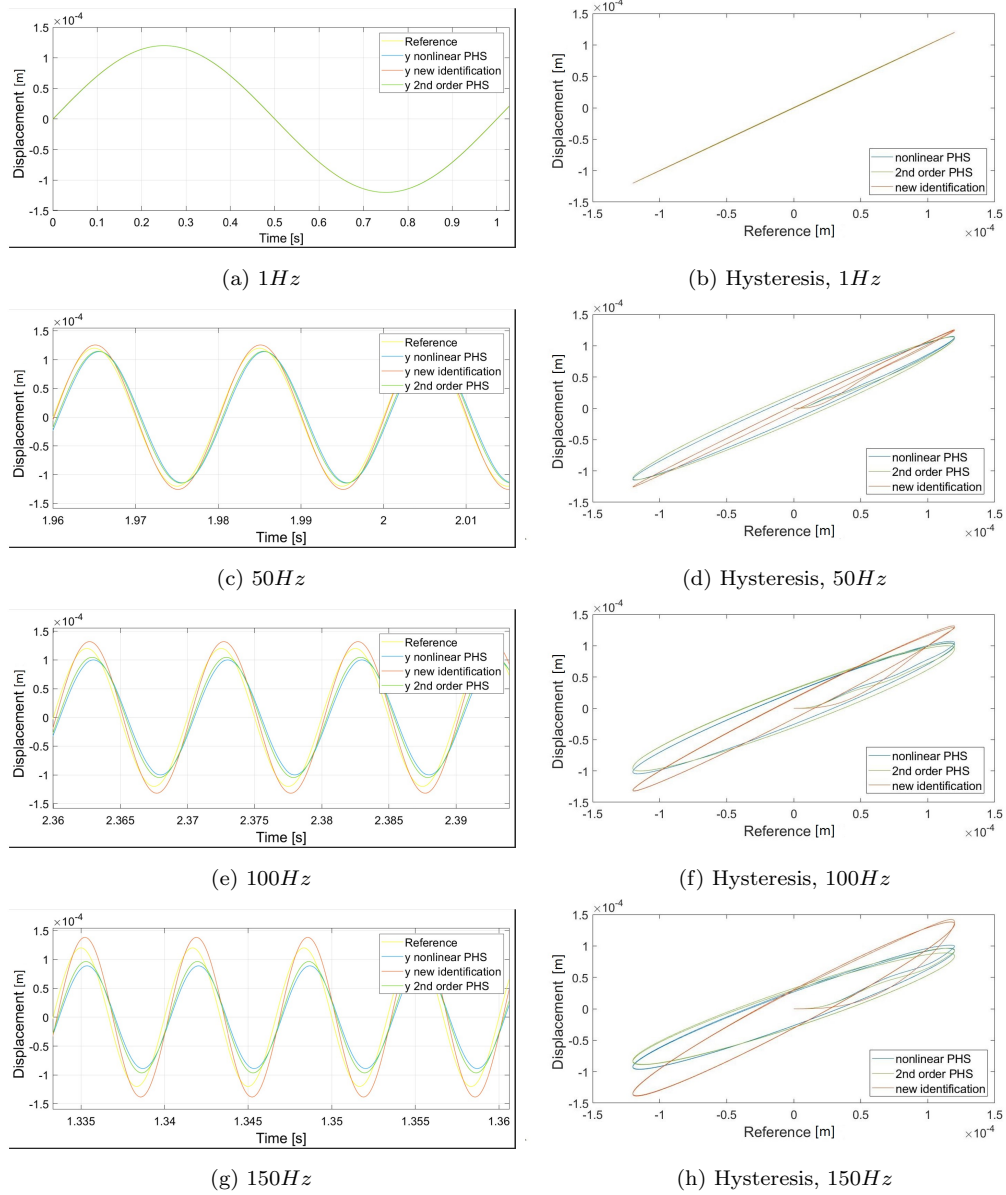


Figure 3.10: Sinusoidal response and Hysteresis

3.3 Global Stability

Since we choose the pole with a negative real part, the local stability is ensured, otherwise the control wouldn't be possible. Let's now analyse the global stability.

We consider the following proposition [4]:

Proposition 3.3.1. *The unperturbed piezoelectric actuator model given by Proposition (2.2.1), by taking $F_{ext} = 0$, when controlled by the control action*

$$u_{in} = V_{in}^* + k_1 e(t) + k_2 \int e(\tau) d\tau \quad (3.28)$$

where $e(t) = r(t) - q(t)$ is the tracking error, $V_{in}^* = \frac{k}{\alpha} r(t)$ is the equilibrium point voltage value when $q^* = r(t)$ assuming $Q_i^* = 0$, and the pair (k_1, k_2) is the gain of the proportional-integral controller; is asymptotically stable to the equilibrium position $q^* = r(t)$ if $\max_i(\rho_i^{-1}) < \lambda_{\min}(Q)/2\lambda_{\max}(PG)$ where ρ_i^{-1} is the linear admittance of the hysteron, $G = \text{diag}(1, \dots, 0, 0, 0)$, P and Q fulfills $PA + A^T P = -Q$ with

$$\mathcal{A} = \begin{bmatrix} A - BK_1 & -BK_2 \\ M & 0 \end{bmatrix} \quad A = \begin{bmatrix} -\frac{\rho_i^{-1}}{C_i} & \dots & 0 & \frac{\alpha}{m} \\ \vdots & \ddots & \vdots & \vdots \\ 0 & \dots & 0 & \frac{1}{m} \\ \frac{-\alpha}{C_i} & \dots & -k & \frac{-b}{m} \end{bmatrix} \quad (3.29)$$

$$B = \begin{bmatrix} 0 & \dots & 0 & \alpha \end{bmatrix}^T$$

where ρ_i^{-1} is the linear slope of the nonlinear hysteron admittance h_i^{-1} , $K_1 = \begin{bmatrix} 0 & \dots & k_1 & 0 \end{bmatrix}$ and $K_2 = [k_2]$, $M = \begin{bmatrix} 0 & \dots & 1 & 0 \end{bmatrix}$.

See [4] for the proof.

We can prove it only with the first PI controller, since for the second one we don't have all the parameters needed. In our case k_1 and k_2 are equal to K_p and K_i found with pole placement method, respectively, and substituting with the values of the table (2.1), the matrices are:

$$A = \begin{bmatrix} -\frac{0.6002}{5.6425 \cdot 10^{-7}} & 0 & 0 & \frac{0.046311}{1.0148 \cdot 10^{-3}} \\ 0 & -\frac{1.1528 \cdot 10^{-4}}{5.2125 \cdot 10^{-7}} & 0 & \frac{0.046311}{1.0148 \cdot 10^{-3}} \\ 0 & 0 & 0 & \frac{1}{1.0148 \cdot 10^{-3}} \\ \frac{-0.046311}{5.6425 \cdot 10^{-7}} & \frac{-0.046311}{5.2125 \cdot 10^{-7}} & -24579 & \frac{-3.7356}{1.0148 \cdot 10^{-3}} \end{bmatrix} \quad B = \begin{bmatrix} 0 \\ 0 \\ 0 \\ 0.046311 \end{bmatrix}$$

$$K_1 = \begin{bmatrix} 0 & 0 & 8.5811 \cdot 10^5 & 0 \end{bmatrix} \quad K_2 = [9.6755 \cdot 10^8] \quad (3.30)$$

The matrix $Q = Q^T > 0$, of the *Lyapunov matrix equation*, is arbitrary and we choose it as an 5x5 identity matrix. Having \mathcal{A} and Q , the matrix

$P = P^T > 0$ is found using the MatLab function *'lyap'*.

The eigenvalues of PG are $(0, 0, 0, 0.022653084227172, 0.000001458464736)$ and the eigenvalues of Q are all 1s, since it is an identity matrix. Now, it is easy to prove that the inequality $\max_i(\rho_i^{-1}) < \lambda_{\min}(Q)/2\lambda_{\max}(PG)$ holds:

$$0.6002 < 1/(2 \cdot 0.022653084227172) \implies 0.6002 < 22.072 \quad (3.31)$$

The controlled system with PI gains $K_p = 8.5811 \cdot 10^5$ and $K_i = 9.6755 \cdot 10^8$ is globally asymptotically stable.

Chapter 4

Experimental Validation

The objective of this chapter is to present the hardware and software setup used for the tests on the real plant. The tests made considering the PI controllers designed in Chapter 3.1. The results show different behaviour of the piezoelectric actuator in response to sinusoidal and step signals for each PI controller. When using the PI controller designed considering the PHS model identified based on sinusoidal response (equation 3.9), the results with sinusoidal inputs outperforms the step input response. Vice versa, when using the PI controller designed considering the model identified on step response (equation 3.15).

4.1 Experimental Setup

The configuration diagram is showed in Figure 4.1 and the experimental setup is showed in Figure 4.2.

The dSpace MicroLabBox (MLB) is the system where input and output signals are processed. Programming is accomplished using the Simulink software from MatLab, combined with dSpace software. The essential components from dSpace software are the ADC Class 1 and DAC Class 1, representing the input and output blocks of the MLB, respectively. The MLB is directly linked to the host PC. Utilizing the Control Desk software provided by MLB, allows real-line monitoring of desired parameters and modification of some parameters during runtime. For this purpose, a Human-Machine Interface

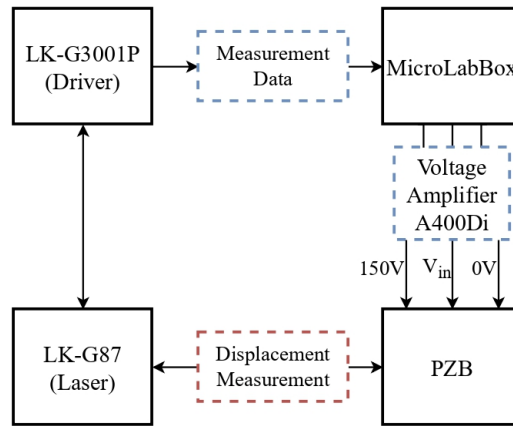


Figure 4.1: Configuration diagram

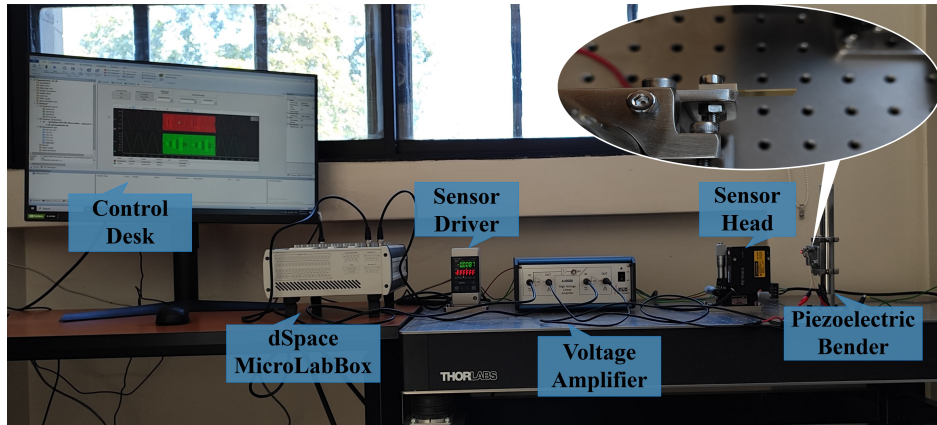


Figure 4.2: Experimental setup

(HMI) is designed in Control Desk (Figure 4.3).

The bender piezoelectric actuator involved is the PB4VB2S from Thorlabs. To drive it an input signal of 150 V is needed, considering that the MLB can output a signal up to 10 V a Voltage Amplifier is needed. The linear voltage amplifier A400DI is used, which has x20 gain with a maximum of 200 V. To drive the PB4VB2S with a bidirectional bending a differential voltage control must be used. This connection strategy is presented in the diagram from Figure 4.4. Noting that, there are two active wires, one that is fixated in 150 V and the other one that drives the actuation signal ranging from 0 to 150 V, both amplification channels from the amplifier are used. The PB4VB2S is connected to A400DI and the A400DI is connected, through

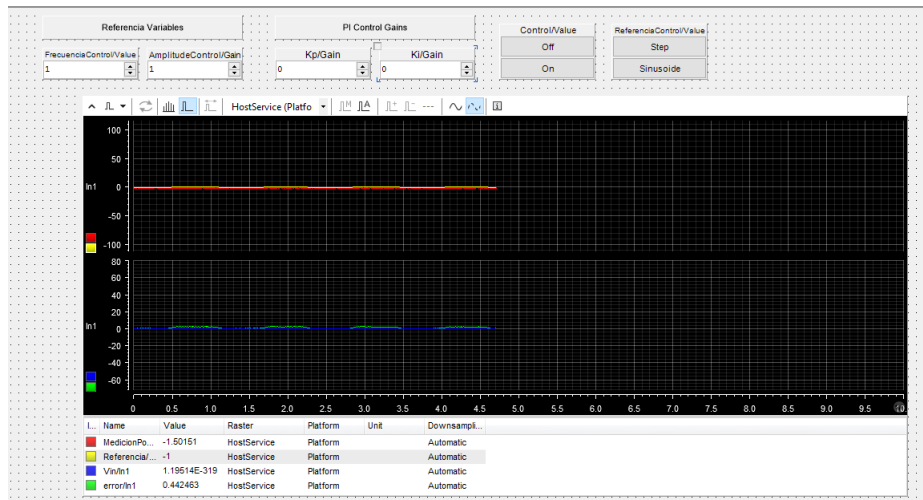


Figure 4.3: HMI - Control Desk

two digital outputs to MLB (Figure 4.4), AO.1 for the constant voltage and AO.2 for the driving one.

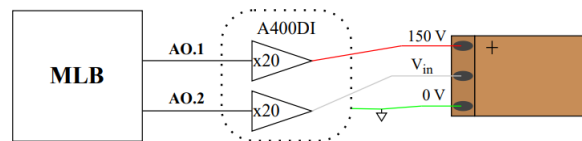


Figure 4.4: Piezoelectric actuator connection configuration

The position is measured using a laser sensor, the LK-G87 sensor head paired to the LK-G3001P driver. It is connected to MLB through a digital input. Following is presented each component involved in the experiments.

MicroLabBox

The dSpace MicroLabBox lets set up the control, test or measurement applications quickly and easily, and helps to turn a new control concepts into reality (Figure 4.5). More than 100 I/O channels of different types make MicroLabBox a versatile system that can be used in mechatronic research and development areas, such as robotics, medical engineering, electric drives control, renewable energy, vehicle engineering, or aerospace. High computation power combined with very low I/O latencies provide great real-time

performance. A programmable FPGA gives you a high degree of flexibility and lets you run even extremely fast control loops, as required in applications such as electric motor control or active noise and vibration cancellation [31]. MicroLabBox is supported by a comprehensive dSPACE software package, including, e.g., Real-Time Interface (RTI) for Simulink for model-based I/O integration and the experiment software ControlDesk, which provides access to the real-time application during run time by means of graphical instruments.



Figure 4.5: MicroLabBox

The bender piezoelectric actuator - PB4VB2S

The PB4VB2S bender actuator consists of a piezoelectric bimorph attached to a specially designed carrier which makes it easier for customers to incorporate (Figure 4.6). The piezoelectric bimorph is co-fired with multiple piezoelectric ceramic layers. This actuator offers a maximum displacement of $\pm 135 \mu m \pm 15\%$. It has three electrodes on the top surface and a silver plus sing is located next to one electrode attached to red wire, which should receive positive bias [8].

The amplifier - A400DI

The A400DI, from FLC Electronics, is a dual general purpose broadband linear amplifier having a fixed amplification of 20 times and capable of bipolar high voltage output of $\pm 200 V$ (Figure 4.7). Any function generator or

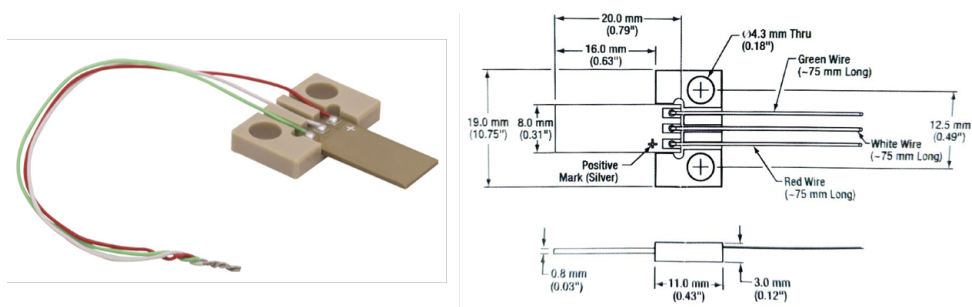


Figure 4.6: PB4VB2S bender piezoelectric actuator

arbitrary waveform generator or any other signal source with amplitude up to $\pm 10\text{ V}$ can be used as an input device. The amplifier's output is linear from DC up to megahertz range. It can be used in a wide range of applications, for example to drive piezo actuators, micro-electromechanical systems (MEMS), organic light emitting diodes (OLEDs), liquid crystals, etc. [32].



Figure 4.7: A400DI amplifier

The position sensor head - LK-G87

The LK-G87 module is a multi-purpose, wide beam sensor head created and manufactured by the KEYENCE Corporation as part of the LK-G3000 series of cameras and camera equipment (Figure 4.8).

The LK-G87 sensor head is a Class II (FDA) and Class 2 (IEC) class of laser. The LK-G87 module's measuring range is $80 \pm$ millimeters long. The repeatability of the LK-G87 module is $0.2\ \mu\text{m}$. Lastly, the spot diameter is $70 \times 1100\ \mu\text{m}$ [33].



Figure 4.8: LK-G87 Keyence sensor head

The position sensor driver - LK-G3001P

The LK-G3001P is a separate monitor model controller that is manufactured by Keyence for the LK-G3000 series (Figure 4.9). The display is compatible with all LK-G sensor heads. Up to two sensors can be connected at one time. The minimum display unit is $0.01 \mu m$. The display range is $\pm 9999.99 mm$ to $\pm 9999.99 \mu m$. The refresh rate is 10 times/second [34].



Figure 4.9: LK-G3001P Keyence sensor driver

4.2 Experimental Tests

First of all we add a saturation block at the output signal in Simulink, to be sure that the maximum voltage ($150V$) allowed for the piezoelectric actuator is not overpassed. While, a low-pass filter is added at the input signal to reduce the noise.

The maximum amplitude applied for the tests is of $110\mu m$. We not consider an amplitude of $120\mu m$, as for the test simulated with Simulink, which is the maximum reachable displacement observed, in order to have margin for controller correction.

In the following plots the blue line is the reference input and the red line is the displacement output.

4.2.1 Step response

Testing the first PI controller (3.14), based on the PHS model, the step response result in Figure 4.10 is quite different from what obtain in the simulation test (see Figure 3.9). A very high overshoot and oscillations are present, even considering the noise contribution. The tests are made with different amplitudes ($30, 70, 110\mu m$) and the behaviour doesn't change. This is due to the fact that the PHS nonlinear model take into consideration it was better identified for sinusoidal response and not for step response (see Chapter 2.3).

Let's tests now the second PI controller (3.16). The step response, for the same amplitude of $30, 70$ and $110\mu m$, is showed in Figure 4.10. The result is as expected, from the plots is clear that no overshoot and no oscillation are present. Even if the fit percentage of this identification (78.25%) is lower than the one obtained for the PHS model (see Table 2.3), the step response is better behaving. This is a confirmation of what we already supposed, that the PHS identification was only taking into consideration the sinusoidal response, while the new identification is based on step response.

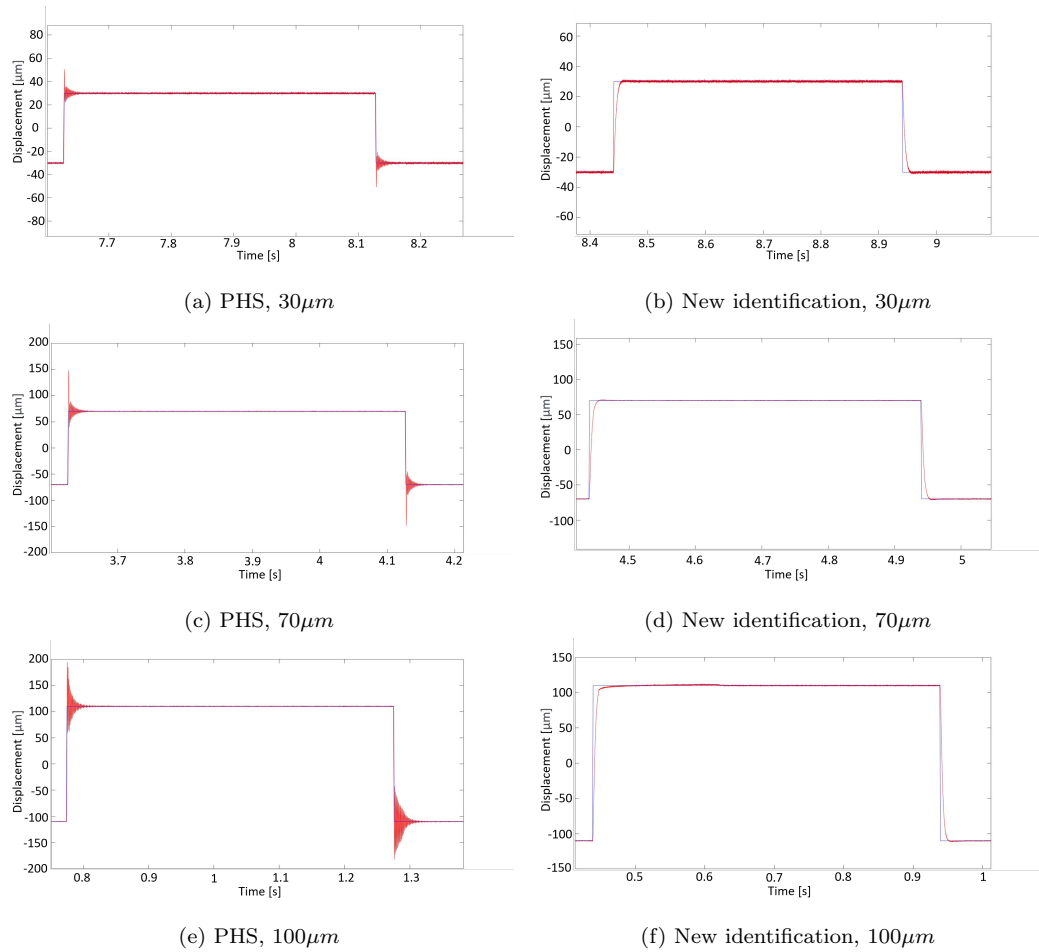


Figure 4.10: Step response

4.2.2 Trajectory tracking

Starting with the first PI controller (3.14), the tests with sinusoidal input are at frequency of 1, 50, 100 Hz, with an amplitude of $110\mu m$. The frequency 150 Hz is the maximum safety working frequency chosen for these experiments, a conservative choice in order to preserve as long as possible the piezoelectric actuator to wear. For this reason the test was done with a smaller amplitude, $15\mu m$. The input-output plots and the hysteresis plots are shown in Figures 4.11 and 4.12. As we find out with the simulation tests in Chapter 3.2, the PI controller is working better at lower frequencies.

For the second PI controller (3.16), the sinusoidal response is showed in

figures 4.11 and 4.12, considering the frequencies 1, 50, 100 Hz with amplitude 70 μm and 150 Hz with amplitude 15 μm . As for the simulation, in sinusoidal response, the PI controller is combined with a feedforward action. The change of amplitude, from 110 μm to 70 μm , is due to the fact that these tests were made during a hotter weather than the previous one, since the piezoelectric actuator is sensitive to the temperature it was not able to perfectly reach high displacements (even with the older PI controller). Therefore, to have comparable results the amplitude was reduced.

Observing the plots, we carry out that the sinusoidal response with the new PI controller and the feedforward is not good as the result obtained with the old PI controller and not feedforward. It is possible to conclude that each PI controller better performs when working with the response type for each its model identification was based on. The 'old' PI controller (see 3.14) for sinusoidal response and the 'new' PI controller (see 3.16) for step response. The hysteresis plots for 150 Hz are compared in Figure 4.12.

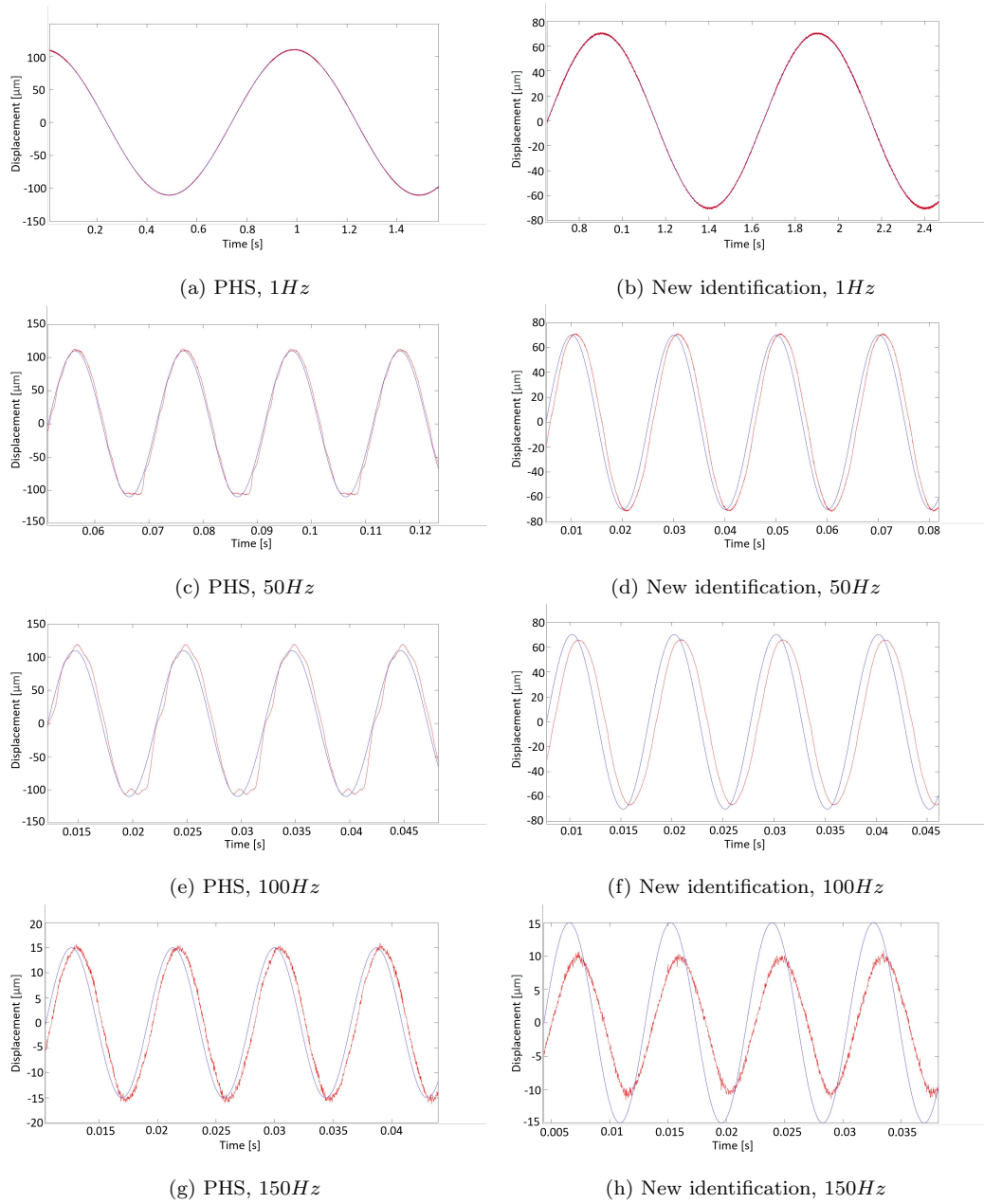
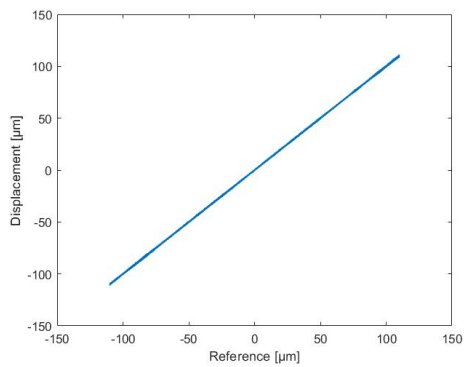
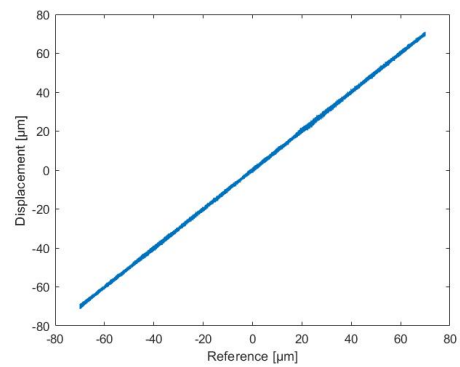


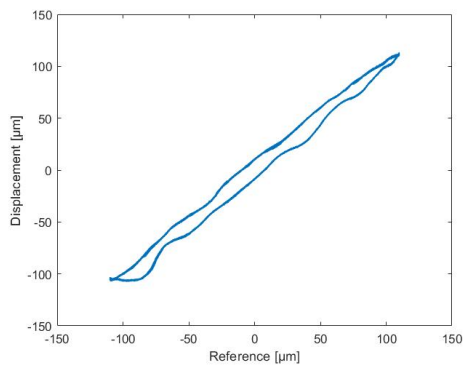
Figure 4.11: Sinusoidal response



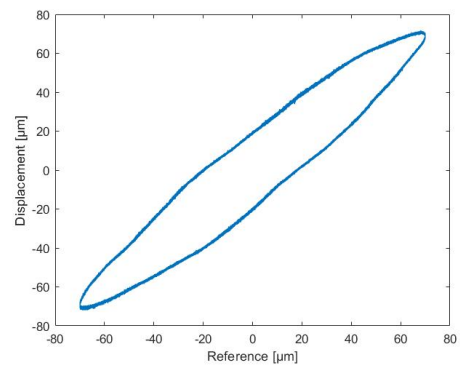
(a) PHS, 1Hz



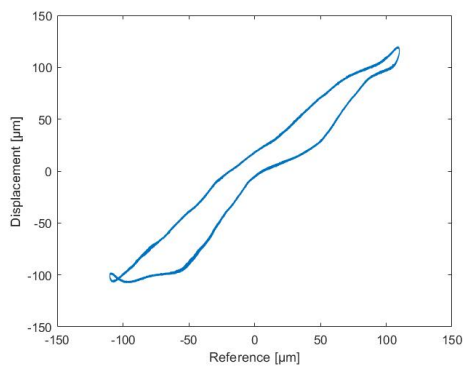
(b) New identification, 1Hz



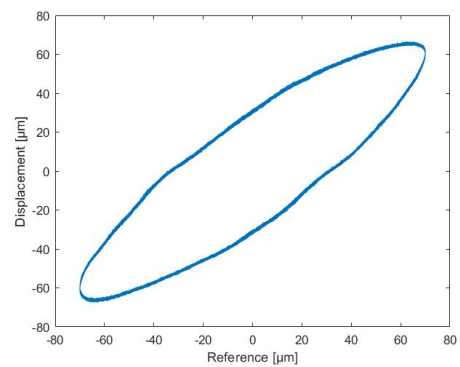
(c) PHS, 50Hz



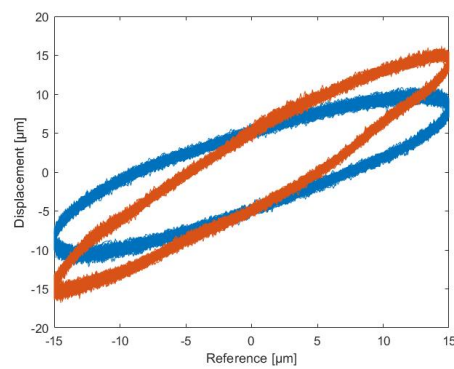
(d) New identification, 50Hz



(e) PHS, 100Hz



(f) New identification, 100Hz



(g) 150Hz, red is PHS and blue is the New identification

Figure 4.12: Hysteresis

Conclusions

Thanks to AC3E, Advanced Center of Electrical and Electronic Engineering of the Federico Santa María Technical University (UTFSM) in Valparaíso, Chile [6], there was the possibility to study piezoelectric actuators. The aim of the thesis was to find a control strategy, easily implementable, for the commercial piezoelectric actuator PB4VB2S [8]. The necessity to control this type of actuators is due to their nonlinear input/output behaviour, represented by the hysteresis. Two PI controller are proposed, one considering a identification model based on sinusoidal response, while the other one considering the identification based on step response.

The model identified on sinusoidal response is a port-Hamiltonian system with a fit percentage over 96.5% (PHS - studied in [4]), where a linearization and an order reduction (from 4th to 2nd) is done, in order to apply a practice procedure for the control design. For the same reason and to have comparable results, the identification for the step response was directly obtained for a 2nd order system with a fit percentage of 78.25%.

The two PI controllers are tested on the real plant, for both step and sinusoidal response at different amplitudes and frequencies. As expected, the results obtained are quite different depending on the input reference. The PI controller designed for the PHS system, better performs for sinusoidal response, while the other PI controller better performs for step response, even with a lower identification fit percentage. Actually, each PI controller better performs when working with the response type for each its model identification was based on. The reasons of this diversity is mainly due to the highly nonlinearity present in the piezoelectric actuator, moreover with the calculation simplification for the PHS system, considering the order reduction, we focus on the mechanical part and not on electrical one, which depends on

the hysteresis.

During the experimental tests was possible to observe how sensitive to temperature the piezoelectric actuator is. The first tests was made during colder season and the last ones in a hotter season. This change of temperature produced a variation in the piezoelectric actuator behaviour, where at higher temperature was very difficult to reach the maximum displacement allowed. Consequently, was not possible to have a perfect repeatable experiment conditions.

Testing the piezoelectric actuator at its displacement limit ($120\mu m$) and at high frequency ($150Hz$), three actuators broke. To preserve the device, displacement and frequency constraint are taken into account.

As future work, it is possible to study the thermodynamic behaviour, in order to better identify the overall piezoelectric actuator dynamics. Adding a temperature sensor, allows us to have an active control to compensate the change of temperature.

Bibliography

- [1] MAS.865, Piezoelectric actuators (2018).
URL <https://fab.cba.mit.edu/classes/865.18/motion/piezoelectric/index.html>

- [2] T.-G. Zsurzsan, C. Mangeot, M. A. E. Andersen, Z. Zhang, N. A. Andersen, Piezoelectric stack actuator parameter extraction with hysteresis compensation, 2014 16th European Conference on Power Electronics and Applications (2014) 1–7.
URL <https://api.semanticscholar.org/CorpusID:18433407>

- [3] H. Mounir, P. Lutz, M. Rakotondrabe, Robust and optimal output-feedback control for interval state-space model: Application to a 2-dof piezoelectric tube actuator, *Journal of Dynamic Systems, Measurement, and Control* 141 (07 2018). doi:10.1115/1.4040977.

- [4] I. DÍAZ, A modular port based model and passivity based control approach for a class of piezoelectric actuators (10 2023).

- [5] S. J. Rupitsch, *Piezoelectricity*, Springer Berlin Heidelberg, Berlin, Heidelberg, 2019, pp. 43–81. doi:10.1007/978-3-662-57534-5_3.
URL https://doi.org/10.1007/978-3-662-57534-5_3

- [6] U. T. F. S. María, *Ac3e* (2023).
URL <https://ac3e.usm.cl/>

- [7] M. E. S. Graham C. Goodwin, Stefan F. Graebe, *Control system design*, Prentice Hall, Upper Saddle River, N.J., 2001.

- [8] Thorlabs, Piezoelectric actuator - pb4vb2s (2023).
URL <https://www.thorlabs.com/thorproduct.cfm?partnumber=PB4VB2S>
- [9] A. Van Der Schaft, D. Jeltsema, et al., Port-Hamiltonian systems theory: An introductory overview, Vol. 1, Now Publishers, Inc., 2014.
- [10] W. P. Mason, Piezoelectricity, its history and applications, The Journal of the Acoustical Society of America 70 (6) (1981) 1561–1566. arXiv:https://pubs.aip.org/asa/jasa/article-pdf/70/6/1561/11924187/1561\1\1_online.pdf, doi:10.1121/1.387221.
URL <https://doi.org/10.1121/1.387221>
- [11] D. Vatansever, E. Siores, T. Shah, Alternative resources for renewable energy: Piezoelectric and photovoltaic smart structures, in: B. R. Singh (Ed.), Global Warming, IntechOpen, Rijeka, 2012, Ch. 10. doi:10.5772/50570.
URL <https://doi.org/10.5772/50570>
- [12] OnScale, What is piezoelectricity? (2023).
URL <https://onscale.com/piezoelectricity/what-is-piezoelectricity/>
- [13] A. Aabid, M. A. Raheman, Y. E. Ibrahim, A. Anjum, M. Hrairi, B. Parveez, N. Parveen, J. Mohammed Zayan, A systematic review of piezoelectric materials and energy harvesters for industrial applications, Sensors 21 (12) (2021). doi:10.3390/s21124145.
URL <https://www.mdpi.com/1424-8220/21/12/4145>
- [14] EL-PRO-CUS, What is a piezoelectric actuator : Working and its applications.
URL <https://www.elprocus.com/piezoelectric-actuator/>
- [15] Y. Mamiya, Applications of piezoelectric actuator, Nec Technical Journal 1 (2006) 82–86.
URL <https://api.semanticscholar.org/CorpusID:44002490>

- [16] H. Wang, Y. An, Z. Wang, H. Li, L. Wen, Simulation of piezoelectric plasma micro-thruster, The 9th IEEE International Conference on Nano/Micro Engineered and Molecular Systems (NEMS) (2014) 622–625.
URL <https://api.semanticscholar.org/CorpusID:42437179>
- [17] J. Vaclavik, P. Mokřý, Measurement of mechanical and electrical energy flows in the semi-active piezoelectric shunt damping system, Journal of Intelligent Material Systems and Structures 23 (2012) 527–533. doi:10.1177/1045389X12436730.
- [18] M. Ju, Z. Dou, J.-W. Li, X. Qiu, B. Shen, D. Zhang, F.-Z. Yao, W. Gong, K. Wang, Piezoelectric materials and sensors for structural health monitoring: Fundamental aspects, current status, and future perspectives, Sensors 23 (1) (2023). doi:10.3390/s23010543.
URL <https://www.mdpi.com/1424-8220/23/1/543>
- [19] J. Li, H. Huang, T. Morita, Stepping piezoelectric actuators with large working stroke for nano-positioning systems: A review, Sensors and Actuators A: Physical 292 (2019) 39–51. doi:<https://doi.org/10.1016/j.sna.2019.04.006>.
URL <https://www.sciencedirect.com/science/article/pii/S0924424719300184>
- [20] Y. Zhang, M. Ourak, E. Verschooten, K. Niu, D. Wu, G. Borghesan, P. Joris, E. Vander Poorten, Controlling of a micropositioning piezoelectric actuator using an lstm network for robotic eye surgery, in: Conference on New Technologies for Computer and Robot Assisted Surgery, Location, 2022.
- [21] H. Llewellyn-Evans, C. Griffiths, A. Fahmy, Microgripper design and evaluation for automated μ -wire assembly: a survey, Microsystem Technologies 26 (06 2020). doi:10.1007/s00542-019-04741-4.
- [22] W. Xu, Y. Wu, Piezoelectric actuator for machining on macro-to-micro cylindrical components by a precision rotary motion control, Mechanical Systems and Signal Processing 114 (2019) 439–447.

doi:<https://doi.org/10.1016/j.ymsp.2018.05.035>.

URL <https://www.sciencedirect.com/science/article/pii/S0888327018302899>

- [23] B. Komati, A. Kudryavtsev, c. clévy, G. Laurent, T. Brahim, J. Agnus, P. Lutz, Automated robotic microassembly of flexible optical components, 2016, pp. 93–98. doi:10.1109/ISAM.2016.7750721.
- [24] Murata, Basic knowledge of microblower (air pump).
URL <https://www.murata.com/en-global/products/mechatronics/fluid/overview/basics>
- [25] J. Gan, X. Zhang, A review of nonlinear hysteresis modeling and control of piezoelectric actuators, AIP Advances 9 (4) (2019) 040702. arXiv:https://pubs.aip.org/aip/adv/article-pdf/doi/10.1063/1.5093000/12850425/040702_1_1_online.pdf, doi:10.1063/1.5093000.
URL <https://doi.org/10.1063/1.5093000>
- [26] J. Caballería, Modeling and Control of Piezoelectric Actuators: An Irreversible port-Hamiltonian approach (2021) 4–13.
URL <https://repositorio.usm.cl/bitstream/handle/11673/52770/m19191862-2.pdf?sequence=1&isAllowed=y>
- [27] F. Ikhouane, J. Rodellar, Systems with hysteresis: analysis, identification and control using the Bouc-Wen model, John Wiley & Sons, 2007.
- [28] Z. Zhang, X. Tian, X. Ge, Dynamic characteristics of the bouc–wen nonlinear isolation system, Applied Sciences 11 (13) (2021). doi:10.3390/app11136106.
URL <https://www.mdpi.com/2076-3417/11/13/6106>
- [29] M. Rakotondrabe, Bouc–wen modeling and inverse multiplicative structure to compensate hysteresis nonlinearity in piezoelectric actuators, IEEE Transactions on Automation Science and Engineering 8 (2) (2011) 428–431. doi:10.1109/TASE.2010.2081979.
- [30] S. S. Rao, Vibration of continuous systems, John Wiley & Sons, 2019.

- [31] dSpace, Microlabbox (2023).
URL <https://www.dspace.com/en/pub/home/products/hw/microlabbox.cfm>
- [32] Pendulum, Amplifier - a400di (2023).
URL <https://pendulum-instruments.com/products/dual-channel-high-voltage-linear-amplifiers/a400di/>
- [33] Keyence, Sensor head - lk-g87 (2023).
URL <https://www.keyence.com/products/measure/laser-1d/lk-g3000/models/lk-g87/>
- [34] Keyence, Driver - lk-g3001p (2023).
URL <https://www.keyence.com/products/measure/laser-1d/lk-g3000/models/lk-g3001/>